sciendo

TRANSACTIONS ON AEROSPACE RESEARCH
4(261) 2020, pp.13-47
DOI: 10.2478/tar-2020-0019
eISSN 2545-2835

NUMERICAL MODELING OF THE RDE

Michal Folusiak[1], Karol Swiderski[2], Piotr Wolanski[3]
[1]Principal Research Engineer, Gexcon AS, Norway
[2]Senior Technical Expert, SST SwissSafeTech AG, Switzerland,
[3]Łukasiewicz Research Network – Institute of Aviation, Al. Krakowska 110/114, 02-256 Warsaw
michal.folusiak@gmail.com • ORCID: 0000-0002-6796-7588
swiderski@sst-plus.swiss • ORCID: 0000-0001-7135-5587
Piotr.wolanski@ilot.lukasiewicz.gov.pl • ORCID: 0000-0003-3963-7722

Abstract

The idea of using the phenomenon of rotating detonation to propulsion has its roots in fifties of the last century in works of Adamson et al. and Nicholls et al. at the University of Michigan. The idea was recently reinvented and experimental research and numerical simulations on the Rotating Detonation Engine (RDE) are carried in numerous institutions worldwide, in Poland at Warsaw University of Technology (WUT) since 2004. Over the period 2010-2014 WUT and Institute of Aviation (IOA) jointly implemented the project under the Innovative Economy Operational Programme entitled 'Turbine engine with detonation combustion chamber'. The goal of the project was to replace the combustion chamber of turboshaft engine GTD-350 with the annular detonation chamber.

This paper is focused on investigation of the influence of a geometry and flow conditions on the structure and propagation stability of the rotating detonation wave. Presented results are in majority an outcome of the aforementioned programme, in particular authors' works on the development of the in-house code REFLOPS USG and its application to simulation of the rotating detonation propagation in the RDE.

Keywords: RDE, CFD, modeling, detonation, numerical.

1. INTRODUCTION

The principle of the RDE is based on propagation of spinning detonation wave in annular chamber. A fresh mixture must have sufficient time, enough to refill the reaction zone, where the detonation wave has already passed, before the next appearance of detonation front. At the same time the combustion products are being exhausted towards a turbine inlet or a nozzle producing thrust for the engine. The working frequency of the engine depends on propagation velocity and chamber's geometry. For example, if internal diameter of the chamber equals 100mm and hydrogen-air mixture is supplied then the working frequency is about 5kHz [1].

The detonation is a phenomenon which has been known for over a hundred years. This process of rapid combustion is generally understood, however the details of the shock structure and chemical mechanism of the detonation is still a subject of intense research due to its practical importance. Recently, the study on the RDE has given a new impulse for science of detonation. Because of the geometrical

complexity of the spinning and rotating detonation, new experimental and numerical tools are needed, in particular robust codes for simulating the rotating detonation engine in complex geometries. Such codes should allow resolving details of the flow field which are unavailable from analysis of the experimental results. What is more, once validated, they could be a useful tool for optimization of the rotating detonation engine in the future.

Since the 1950s numerical methods based on the Euler equations have been developed to predict flows with discontinuities. For their approximations, the Finite Volume Method (FVM) in conjunction with Riemann solvers permits shock capturing.

Nowadays rotating detonation has become a subject of numerical research at many institutions all over the world. The performance aspects of the RDE as well as the effect of changing the injection pressure or nozzle shapes have been investigated by Chinese researchers, Shao et al [2], [3] and S.J. Liu et al [4]. They have found that the de'Laval nozzle has the best performance (1750 s gross specific impulse) if compared to the converging (1600 s) or diverging nozzle (about 1700 s) or even constant area nozzle (1540 s).

The three-dimensional simulations performed by M. Liu et al [5] for premixed stoichiometric hydrogen-air mixture have uncovered some interesting properties of rotating detonation wave. The authors used one-step chemical kinetics model in their simulation model with a grid size lower than 0.5 mm. If the chamber depth is small the difference between the results at the inner and outer wall is not significant therefore in this case performing 2D simulations should be enough to obtain reasonable results. However, if the chamber height is larger, then the wave pattern is more complex in radial direction and only 3D simulations may be able to provide reliable results. Moreover it was also observed that chamber depth has no effect on detonation height as well as if the chamber depth is higher, the cycle period increases a little bit, and maximum pressure of the flow field increases linearly (see Figure 1).

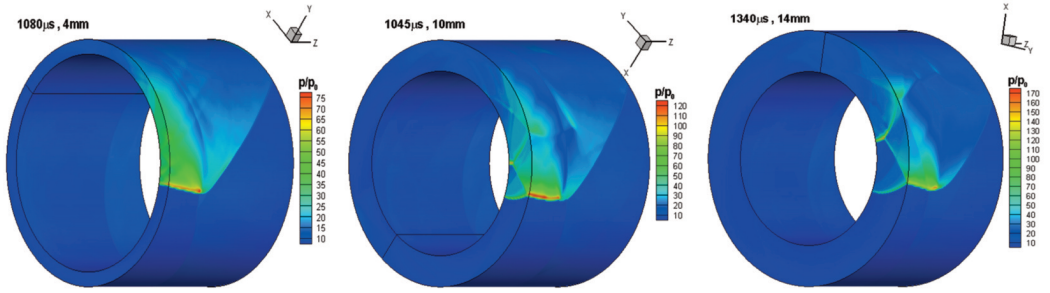

Fig. 1. Chamber depth influence on wave pattern in radial direction. Contours of pressure ratio. Total pressure of the incoming hydrogen-air mixture p_0=25 atm.

A great number of numerical efforts have been made in France by Davidenko et al [6]–[9], especially with a focus on a comparison of the RDE to a conventional rocket engine. Moreover they used 6 species with 7 reactions chemical reactions mechanism for stoichiometric hydrogen-oxygen mixture to investigate the effects of injection pressure and injector relative area. The numerical model employed Euler equations and WENO scheme for the reconstruction of the solution. It was found that the propagation velocity of the detonation wave was equal CJ velocity and was also independent from the chamber height.

The theoretical and computational aspects of the RDE have been investigated in Japan, and have been concerned with studying the limits of detonation operation (Hayashi et al [10]). Hishida et al [11] have investigated the structure of detonation wave in the RDE through detailed numerical analyses and have discovered Kelvin-Helmholtz instabilities and cell structures in the RDE chamber. Some collaborative works have been also made in order to compare the numerical results with experiments performed by Polish researchers, Kindracki and Wolanski [12].

Singaporean and Polish researchers have also conducted some numerical research in the field of the RDE. They have investigated primarily the flow field in the RDE chamber (Folusiak et al [13]) as well as the effects of various nozzle shapes (Yi et al. [14]). Two and three dimensional simulations have been performed using AMR. A simple one-step chemical mechanism for hydrogen-air mixture was used. For both cases the detonation wave propagated with the speed close to CJ velocity. The conclusion was also that since the flow is supersonic at the chamber exit, there was no need to attach a convergent-divergent nozzle.

Moreover, in the United States, independent numerical research has been conducted. Schwer et al developed a numerical procedure to investigate the flow field in the RDE [15] and then performed numerical analyses of flow propagation upstream into the mixture plenum [16]. They have found that the height of the detonation wave generally decreases with decreasing pressure ratio between the inlet and outlet section. Furthermore they have also noticed that mass flow depends mostly on the inlet stagnation properties. Nordeen et al investigated the thermodynamics of detonation wave in the RDE [17], [18]. Lately the performance aspects of the RDE utilizing hydrogen and hydrocarbon fuels have been also investigated by Schwer et al. [19].

Modern classical jet and rocket engines have almost reached a level of development where it is very difficult to increase their performances by minor modifications or just improving the material parameters. In order to achieve significant increase in thermal efficiency of such engine some extraordinary steps must be applied, e.g. change of the thermodynamic cycle of the engine. This goal can be achieved by using detonation mode of combustion instead of deflagration. Detonative combustion can be realized in various ways, for example: by application of pulsed detonation process in so called Pulsed Detonation Engine (PDE), or continuously rotating detonation in the RDE. Advantages of PDE are: relatively simple design and high efficiency. The disadvantages are: small frequency, a necessity of initiation of each cycle, long length and initiation distance, variation of thrust, high level of noise and intensive vibrations. On the other hand, the detonation wave in the RDE, once initiated can propagate continuously in an annular chamber. The engine is more compact and efficient. Smaller variations of thrust are created. There is also a possibility of reducing NOx emission by use of fuel lean mixtures which can burn at lower temperature compared to that obtained in stoichiometric region of combustion in classical burners.

Since the detonation is a combustion process in a constant volume, efficiency of the thermodynamic cycle is higher and there is potential to increase overall efficiency of the engine by order of 10%. The challenge in the RDE engine project is realizing the efficiency of the detonation cycle. Because the detonation wave propagates azimuthally around an annular combustion chamber, the kinetic energy of the flow can be held to a relatively low value and thus the RDE may use most of the compression to increase the efficiency. More information on RDE and detonative propulsion can be found in the works of Wolanski et al [20]–[22].

2. MATHEMATICAL MODEL

The semi-ideal gas model is used in REFLOPS USG. The gas is multi-component with n_{sp} number of components:

$$\frac{p}{\rho} = RT \qquad \rho = \sum_{i=1}^{n_{sp}} \rho_i \qquad y_i = \frac{\rho_i}{\rho} \qquad R = \sum_{i=1}^{n_{sp}} \frac{y_i}{W_i} R_u \tag{1}$$

where specific heat, enthalpy and entropy of the gas components can be described as functions of temperature:

$$c_{pi}(T) = R \sum_{j=1}^{5} \alpha_{ij} T^{j-1} \tag{2}$$

$$h_i(T) = RT\left(\sum_{j=1}^{5}\alpha_{ij}T^{j-1} + \frac{\alpha_{i6}}{T}\right) \tag{3}$$

$$s_i(T) = R\left(\alpha_{i1}\ln(T) + \sum_{j=2}^{4}\frac{\alpha_{ij}}{j-1}T^{j-1} + \alpha_{i7}\right) \tag{4}$$

where α_{ij} are coefficients taken from JANAF tables. The temperature is calculated from:

$$\sum_{i=1}^{n_{sp}}\rho_i h_i(T) - \rho e = \sum_{i=1}^{n_{sp}}\rho_i R_i(T)T \tag{5}$$

Gas dynamics is expressed by Euler's equations:

$$\frac{\partial}{\partial t}\int_V \boldsymbol{U}\,dV + \int_A \vec{\boldsymbol{F}}(U)\cdot\vec{\boldsymbol{n}}\,dA = \int_V \boldsymbol{S}\,dV \tag{6}$$

where $\boldsymbol{U} = \begin{bmatrix}\rho\\ \rho u\\ \rho v\\ \rho w\\ E\\ \rho_i\end{bmatrix}$, $\vec{\boldsymbol{F}}(\boldsymbol{U})\cdot\vec{\boldsymbol{n}} = \begin{bmatrix}\rho\hat{u}\\ \rho\hat{u}u + pn_x\\ \rho\hat{u}v + pn_y\\ \rho\hat{u}w + pn_z\\ \hat{u}(E+p)\\ \rho_i\hat{u}\end{bmatrix}$, $\boldsymbol{S} = \begin{bmatrix}0\\0\\0\\0\\0\\ \dot{\omega}_i\end{bmatrix}$.

Equations are solved on unstructured finite volume grids, fluxes $\boldsymbol{F}$ are determined using one of the available Riemann solvers.

The source term $\boldsymbol{S}$ is chemical composition change rate resulting from the chemical reactions. The production rate of chemical compounds $\dot{\boldsymbol{\omega}}_i$ is an overall sum of the production and destruction rates for a given chemical compound in all reactions taken into account in the chemistry model:

$$\dot{\omega}_i = \frac{d\rho_i}{dt} = W_i\left[\sum_{k=1}^{m}\pm\nu_{i,k}\alpha\left(k_{k,for}\prod_j C_j^{\upsilon_{jk}} - k_{k,back}\prod_j C_j^{\upsilon_{jk}}\right)\right] \tag{7}$$

where:

W_i – i-th specie molar mass
$\nu_{i,k}$ – i-th specie stoichiometric coefficient in k-th reaction
$\alpha = \sum C_j\alpha_{j,k}$ – third body coefficient describing collision of three molecules
$k_{k,for}$ – forward reaction rate
$k_{k,back}$ – backward reaction rate
C_j – j-th specie concentration
υ_{jk} – exponent for j-th specie in k-th reaction

The rate of the reactions is described by the Arrhenius equation:

$$k_{k,for} = A_k T^{n_k}\exp\left(-E_{a,k}/RT\right) \tag{8}$$

whereas the rate of backward-reactions is taken from the assumption of temporary, local thermodynamic equilibrium:

$$K_k = \frac{k_{k,for}}{k_{k,back}} (RT)^{\Delta\nu_k} \tag{9}$$

where:

$$\ln K_k = \frac{\pm\nu_{i,k} s_i^o}{R} - \frac{\pm\nu_{i,k} \Delta h_{f,i}^o}{RT} \tag{10}$$

$E_{a,k}$ is an activation energy of the k-th reaction, A_k pre-exponential constant of the k-th reaction, n_k the temperature exponent of the k-th reaction.

Most fluid flows, especially those in combustion chambers, are turbulent. A key feature of a turbulent flow is a small-scale, high-frequency random fluctuation acting on a main flow. In typical situation, the magnitude of fluctuation is in the range between 5-10% of the main flow magnitude. Such irregularity has a certain impact on the nature of the flow.

The Standard high-Re k-ε turbulence model is based on the two model transport equations for the turbulence energy (k) and its dissipation rate (ε). The modelled RANS equations may be expressed in the following form:

$$\frac{\partial}{\partial t}\int_V \underbrace{\mathbf{U}}_{\substack{\text{vector of}\\ \text{conserved}\\ \text{variables}}} dV + \sum_{j=1}^{N_{faces}} \underbrace{\mathbf{T}}_{\substack{\text{transformation}\\ \text{matrix}}}{}^{-1} \int_{A_j} \left(\underbrace{\mathbf{F}^j}_{\substack{\text{vector of}\\ \text{convective}\\ \text{flux at face j}}} - \underbrace{\mathbf{G}^j}_{\substack{\text{vector of}\\ \text{diffusive (viscous)}\\ \text{flux at face j}}} \right) dA_j = \int_V \underbrace{\mathbf{H}}_{\substack{\text{viscous source}\\ \text{term for}\\ \text{k-}\varepsilon \text{ model}}} dV + \int_V \underbrace{\mathbf{S}}_{\substack{\text{source term}\\ \text{for chemistry,}\\ \text{injection etc.}}} dV \tag{11}$$

Implementation details are omitted here, please refer to [23] for further information.

3. ADAPTIVE MESH REFINEMENT

The Adaptive Mesh Refinement (AMR) is a technique used to speed up numerical simulations on computational grids. The ability of the code to obtain moderately accurate results in a reasonable time is crucial during the design process of combustion chamber, since only readily available results may be useful in decision-making process.

The speedup in AMR is achieved through dynamic refinement of computational grid in regions of high numerical errors. In most transient cases, no prediction of regions of erroneous solution can be done. Thus, ideally refined grid cannot be provided at the stage of building of the computational model for simulation. As a consequence, the use of AMR is advantageous in rotating detonation simulations, since the refinement of the grid is done adaptively each single or several time steps. The refined grid 'follows and keeps up' with the solution providing higher grid resolution and accuracy in regions of high numerical error. The profit can be seen in two ways; either a speedup of solution comparing to the fully refined grid or as an increase of the overall accuracy of the solution.

The AMR approach selected for implementation in REFLOPS USG is similar to other implementations of AMR on unstructured grids. The method does not involve grid clustering as it is done on structured grids in the original method of Berger and Oliger [24], but each cell of the mesh is refined separately. This technique was successfully applied to many CFD codes to date, including [25]–[29].

3.1. Data structure

The selected method of Adaptive Mesh Refinement assumes that elements of the grid are kept in an oct-tree data structure with as many roots as there are elements in the top level (base) mesh and as many branches as there are child elements for each parent element. The selected algorithm of subdivision forces each element in the mesh to have either 8 child elements or none. REFLOPS USG is natively three-dimensional, and the only available element types are three-dimensional 8-node bricks and 4-node tetrahedrons.

In REFLOPS USG, only isotropic refinement, adopted form structured grids algorithms, is possible. Elements are always refined into geometrically similar elements, if any of its faces were flagged or the element was flagged itself. The consequence of this method is production of so-called hanging nodes (Figure 2), that arise at interfaces between two regions of different level of refinement. Such boundaries on one hand require special treatment during flux computation and time update, on the other they greatly simplify the algorithm of refinement.

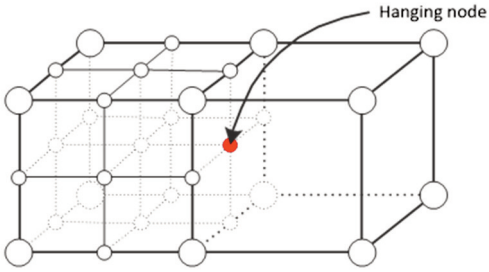

Fig. 2. Hanging node at the interface of two AMR levels.

3.2. Time stepping

The proposed AMR algorithm assumes isotropic subdivision of each element. Therefore, if we assume that all elements in the domain are of similar size, subdivided elements will require about two times smaller time step than parent elements. The consequence of the stability criterion is that Adaptive Mesh Refinement delivers both spatial and temporal refinement. This feature of the AMR algorithm may be seen as a disadvantage, however proper construction of the time stepping algorithm minimizes the additional computational cost.

In the simplest case, the above requirement is not overridden – there is no discerning of elements requiring different time steps and all elements are integrated with the same time step. The algorithm of such procedure is then very similar or even identical to the regular time stepping algorithm. This method is however used very rarely [28], because local Courant number in most computational cells is then unnecessarily lowered.

The other method, that minimizes the disadvantage of temporal refinement, was proposed for the very first AMR algorithms [24], [30] and is widely used for both structured [31] and unstructured meshes [25], [32]. The 'local time stepping' method requires construction of sophisticated time marching algorithm that becomes a recursive sequence of procedures that operate on each grid level separately until the desired point in time for each level is reached. The inter-level synchronization must be ensured each time step and additionally each sub-step of the algorithm. The time step for each level is determined separately before the solution at this level is advanced.

The modification of the above method used in REFLOPS USG is called 'lock-step' algorithm [25] and consists in performing exactly two time steps for every single time step of lower level mesh.

This modification is a consequence of considerations about time step size for refined elements mentioned earlier. The minimum time step size is computed once for each base level time step from the equation:

$$\Delta t_{\min} = \min_{level}\left(\left(\Delta t_{level}\right)_{\min} \cdot 2^{level}\right) \tag{3.1}$$

where $\left(\Delta t_{level}\right)_{\min}$ stands for time step computed according to the CFL stability criterion for single AMR level. The time step that should be used in time marching algorithm for each AMR level becomes:

$$\Delta t_{level} = \Delta t_{\min} \cdot 2^{-level} \tag{3.2}$$

During single time step of base level $\Delta t_0 = \Delta t_{\min}$ algorithm performs 2^{level} steps for each higher level according to the predefined sequence presented in Figure 3.

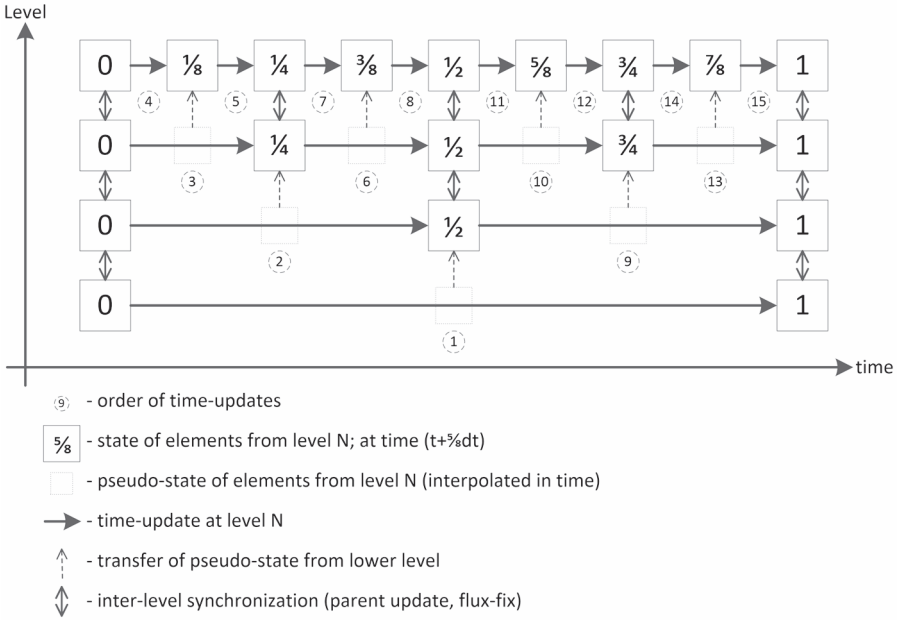

Fig. 3. Time stepping procedure with 3 levels of refinement.

The 'lock-step' time marching algorithm implemented in REFLOPS USG is shown in Figure 3. The rule of thumb is that coarser levels are always updated before their finer counterparts. For each domain of any level algorithm performs four steps. First, data from elements which are overlapped by 'ghost cells' of finer mesh are used to interpolate pseudo-states at half time step of the current grid. Then fluxes that will be used for solution update are computed. Before proceeding to the next step, flux values are stored for the further flux-fix procedure in outer inter-level interfaces. Finally, the solution at current level is advanced by the respective time step. If the current level is the highest level available, the described 4-step procedure is executed one more time. Otherwise it is executed for the higher level. If any of the levels was computed twice, projection of the solution is performed and flux fix procedure is called. Then the 4-step algorithm is called for the lower level. The whole algorithm proceeds until the flux fix procedure is executed for the base level.

3.3. Flux evaluation

In most practical AMR implementations, the so-called nesting requirement is applied during refinement procedure and stands that the level of refinement of two neighbors cannot differ by more than one. Without this requirement, the algorithm of refinement and time marching would be far more complicated. As a result, there are only 3 possible configurations of single element's neighborhood – element can abut element from the same, lower or higher AMR level. The selected AMR algorithm accepts hanging nodes and hanging edges; therefore special treatment must be implemented to the original numerical scheme in order to deal with abutting faces of different size.

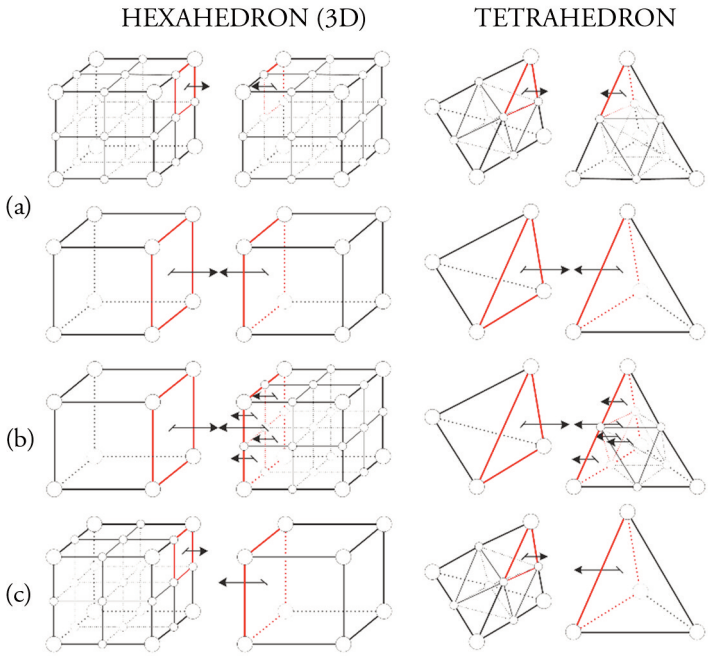

Fig. 4. Time stepping procedure with 3 levels of refinement.

No special treatment is needed in case shown in Figure 4 (a) – this is the only trivial case and it allows direct application of the regular numerical scheme. The other two cases represent inter-level boundaries across which the numerical scheme is modified. If the element abuts elements of higher resolution or in the other words element from the same level which is refined, the flux is evaluated between two elements from the same level. The neighbor element is overlaid by child elements, so the state it stores is projected before the flux is evaluated. Note, that despite the fact the flux computed in such a manner will be used to advance the solution on current level, both the flux and the solution will be further corrected by the flux fix procedure. This will guarantee the conservation at grid interfaces [33]. The reason why this 'coarse' flux is evaluated and the solution updated is that this non-conservative solution is used to determine pseudo-state in ghost cells of higher level grids.

The third and the last case is the inverse of the previous one and is shown in Figure 4 (c) – element of interest abuts element from lower level. Such situation is indicated by the special boundary condition which is assigned by the procedure that generates AMR structure.

More details on flux evaluation and flux-fix procedure can be found in [34].

3.4. Flagging

Flagging is the process of marking elements and its lower topologies with flag parameter. The flag is usually a logical or integer value defined for each element, inter-element boundary (face) and edge. The result of flagging should explicitly and completely describe the new topology that will be built during physical refinement process.

The concept of the Adaptive Mesh Refinement is to increase the overall accuracy through refining regions where large errors in the solution occur, typically regions of high gradients, near discontinuities. Since the general solution of Euler equations are waves which are traveling across the computational domain with finite speeds, any good flagging criterion of Adaptive Mesh Refinement method for hyperbolic equations will detect such discontinuities and refine computational domain in the proximity of these waves. It may be said that mesh refinement should propagate with the discontinuity. On the other hand, the wave is leaving many refined elements in its wake. These elements tend to unnecessarily slow down the computations of considered problem. Therefore any efficient implementation of Adaptive Mesh Refinement method must contain also coarsening mechanism. The derefinement has to travel with the discontinuity likewise, deleting unnecessary elements.

The error analysis cannot be done on-the-fly, since neither the exact nor the fine reference solution is known in practice. Therefore, flagging criterions, which are used to identify faces or elements that require grid refinement, are usually based on the scalar variable gradients across the inter-element boundary. Detailed discussion of other flagging criterions, including error estimate of Richardson or on the Riemann problem properties can be found in [34].

The process of derefinement is usually coupled with refinement process and controlled by the same flagging mechanism. In the case of coarsening, the criterion is met if gradient or wave strength or any selected property is lower than predefined threshold. Such face or element is flagged for deletion.

The process of flagging is governed by the 3 user-defined parameters:
- ε_R – refinement threshold, the sensitivity to refinement;
- ε_D – derefinement threshold, the insensitivity to derefinement (usually two times lower than ε_R);
- maximum AMR levels allowed.

The criterion variable is evaluated for each face or each computational element.

In most AMR algorithms there is additional flagging step which is performed before secondary flagging. Unless flagging and refinement is carried out every time step, the flagging algorithm needs to leave a buffer zone around each level of flagged elements in order to guarantee that flow features, which are assumed to be properly resolver only by the finer mesh, will not move out of the refined region in the meantime. The size of the buffer zone is usually adversely proportional to the frequency of refinement. This simple relation must be again applied with care, since the nonlinearity of PDEs discretized over the mesh may lead to undershoots of the maximum wave speed, which may cause instabilities.

The last step of the flagging process is so-called secondary flagging. The flagging pattern of the domain is modified until the nesting criterion is satisfied. The general rule is that refinement is predominant over derefinement, and therefore the value of flag variable can only be increased.

4. CODE VERFICATION

Six verification tests have been performed and acceptable results were obtained [23]:
- Modified Sod test in 1D (results compared to exact solution, shown in Fig. 5.)
- Explosion in 2D (results compared to REFLOPS1, shown in in Fig. 6.)
- Nozzle flow (results compared to Ansys Fluent, shown in in Fig. 7.)
- Woodward-Colella test (shown in in Fig. 8.)

- Shear flow test (results compared to Ansys Fluent, shown in in Fig. 9.)
- Mach 3 wind tunnel with a step (results compared to various sources, shown in Figures 10, 11, 12 and 13)

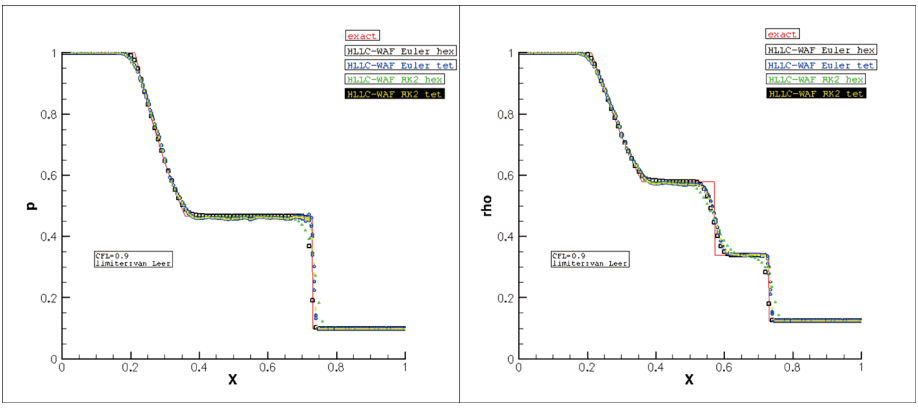

Fig. 5. HLLC-WAF Riemann solver applied to Sod test. Left: Pressure plot. Right: Density plot.

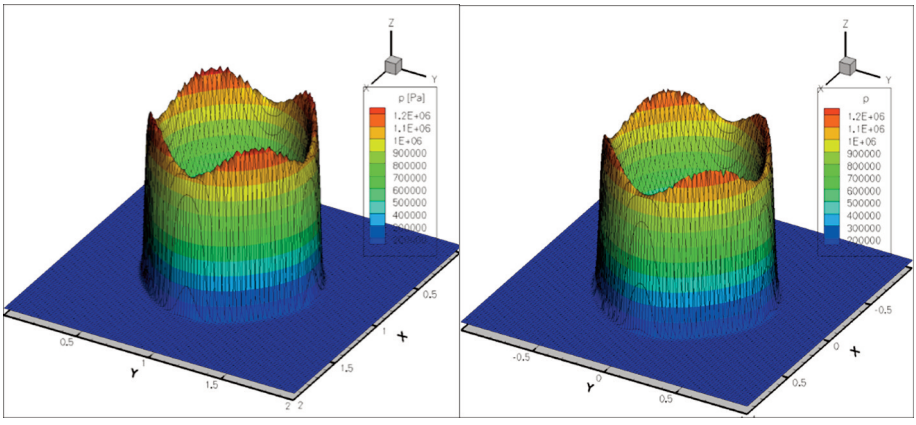

Fig. 6. Explosion test. Pressure plot. Left: REFLOPS1. Right: REFLOPS USG.

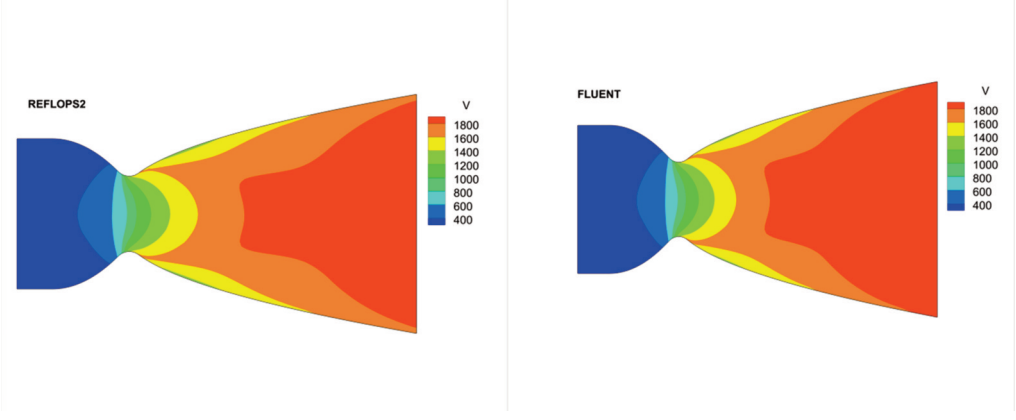

Fig. 7. Nozzle flow velocity magnitude; Left: REFLOPS USG. Right: Fluent. SI units.

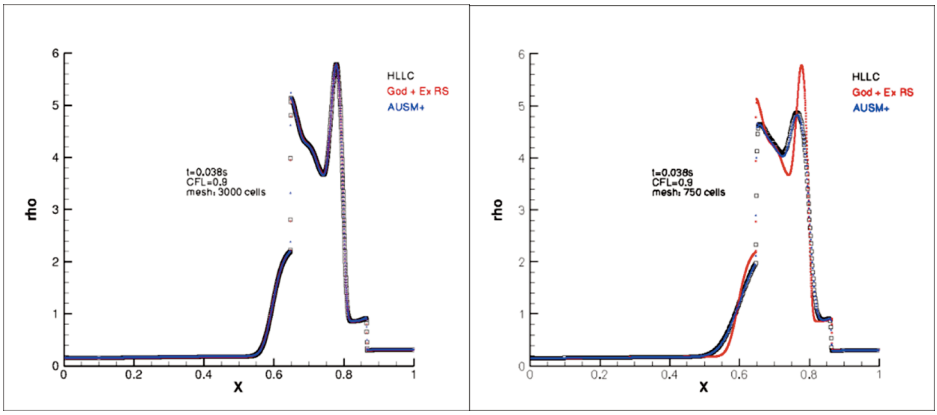

Fig. 8. Woodward and Colella test. Left: fine mesh. Right: coarse mesh.

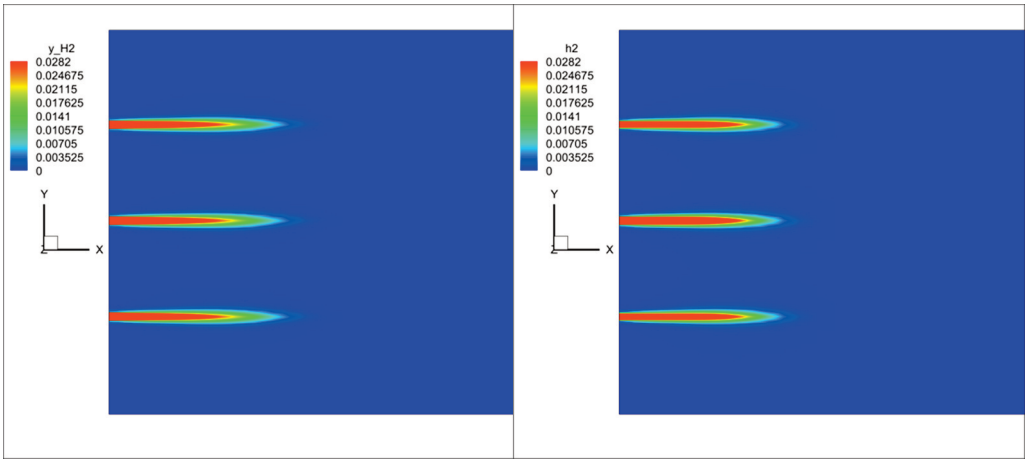

Fig. 9. Contours of H2 mass fractions at the Z=0.06 m plane. The upper value of the scale is stoichiometric level. Left: REFLOPS USG. Right: Fluent.

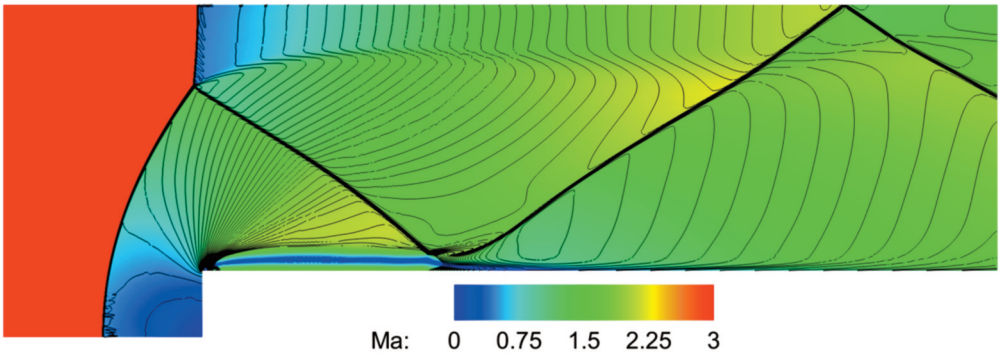

Fig. 10. Mach number contours and density lines. HLLC solver. 3-stage AMR on coarse mesh.

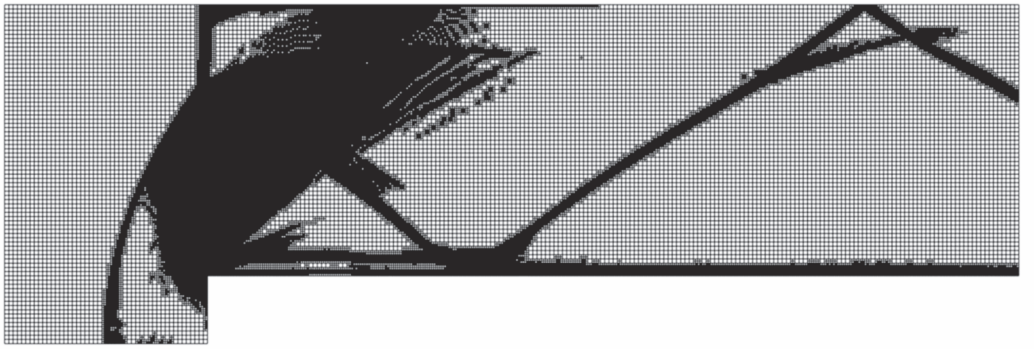

Fig. 11. Mesh adapted at the time level of 4 s. 236439 cells.

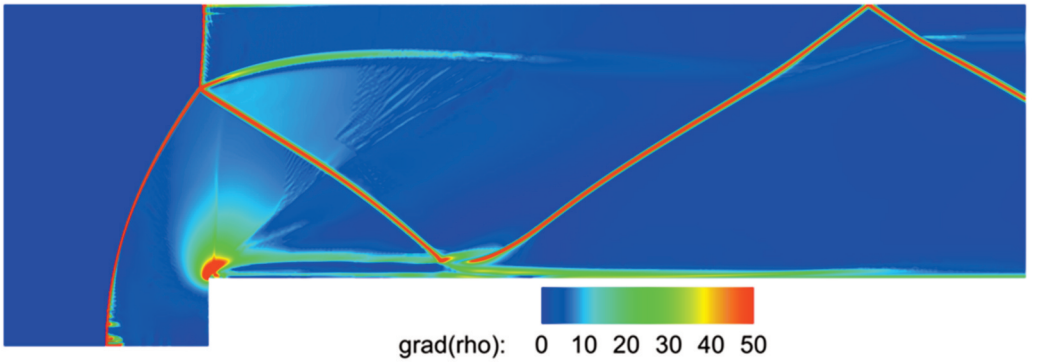

Fig. 12. Density gradient in a low scale [kg/m^4]. HLLC solver. 3-stage AMR on coarse mesh.

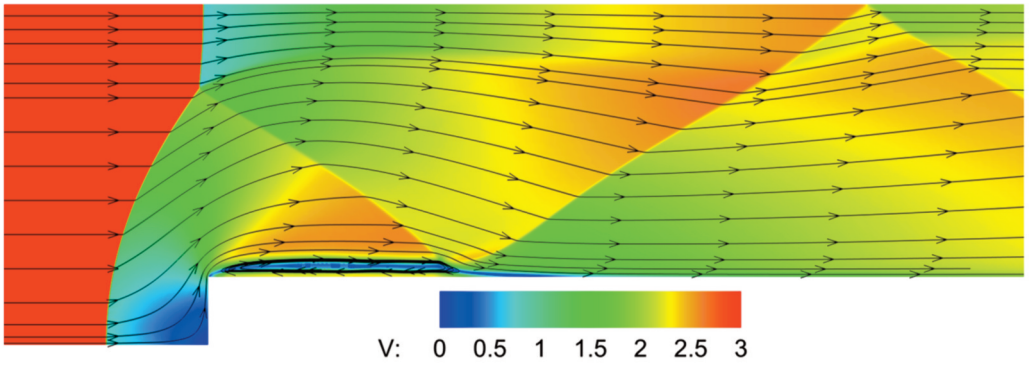

Fig. 13. Velocity magnitude contours [m/s] and streamtraces of the flow. HLLC solver. 3-stage AMR on coarse mesh.

5. CFD SIMULATIONS OF RDE

5.1. Key aspects of RDE simulations

Chemistry kinetics of hydrogen

Detailed combustion mechanisms involving hundreds of species and reactions are not practical for large scale simulations, especially of propulsion systems. Therefore many reduced kinetics mechanisms have been developed for detonation in hydrogen [35]–[37] and hydrocarbon fuels [38] to date. The simplified mechanism is built in a way to assure that the key parameters of detonation match that of detailed mechanism in a range of thermodynamic parameters of interest.

Despite the multiple-step reaction models allow to mimic sophisticated processes of realistic mechanisms, the most common chemical reaction kinetics model is one-step global mechanism. In the presented simulations the numerical cost was the driving factor and a single-step global reaction mechanism was chosen [39]:

$$2H_2 + O_2 = H_2O + H_2O \quad E_a = 1.2e4 \frac{cal}{mole} \quad n = 0 \quad A = 2e17\left(mole, cm, s, K\right) \tag{12}$$

This mechanism was checked against the Petersen's 21-reaction mechanism [37] in case of 1D simulation of propagating detonation wave.

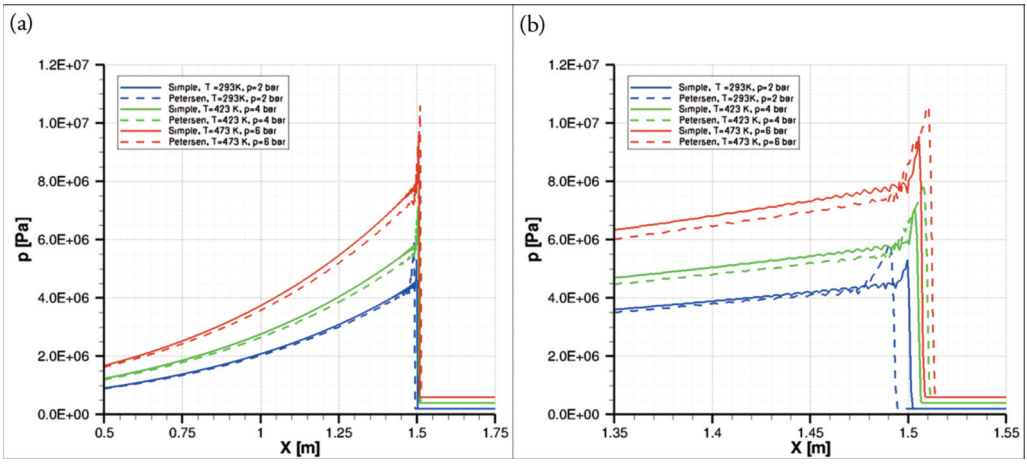

Fig. 14. Comparison of chemical reaction mechanisms: (a) simple and of Petersen; (b) magnified nearby pressure peak.

As shown in Figure 14, the differences between results of both mechanisms are relatively small. The discrepancies manifest mainly in the vicinity of the leading shock and vanish in farther distance from the shock.

Initiation of rotating detonation

Numerical experiments on the initiation of rotating detonation in the RDE combustion chamber have shown [12], that if no special treatment is introduced, the initiation of stable detonation wave is hardly possible in reasonable computational time. At the early stage after numerical ignition the chaotic pattern of multiple detonation waves is created. These are being extinguished, reignited and are interfering with each other until some waves disappear and single or multiple stable detonation waves are created. Such case is illustrated by contour plots of pressure field of unstable detonation and single stable detonation wave shown in Figure 15.

In order to avoid this unfavourable effect, efficient method of initiation of numerical rotating detonation has been developed. The ignition is accomplished with a numerical ignition region of preheated mixture with optionally prescribed circumferential velocity. Only half of the circumference of the combustion chamber is initially activated for chemical reactions, chemical source terms in governing equations are supressed in the other half. The spherical region of ignition is placed at the intersection of these two halves. In such a way, only one detonation wave and one strong shock wave running in opposite directions are obtained. Subsequently, chemical reactions are activated in second half of the domain before detonation wave reaches it. The ignition method succeeds, if after activation of chemical reactions in this region, shock wave is weak enough not to ignite the mixture and generate second detonation wave.

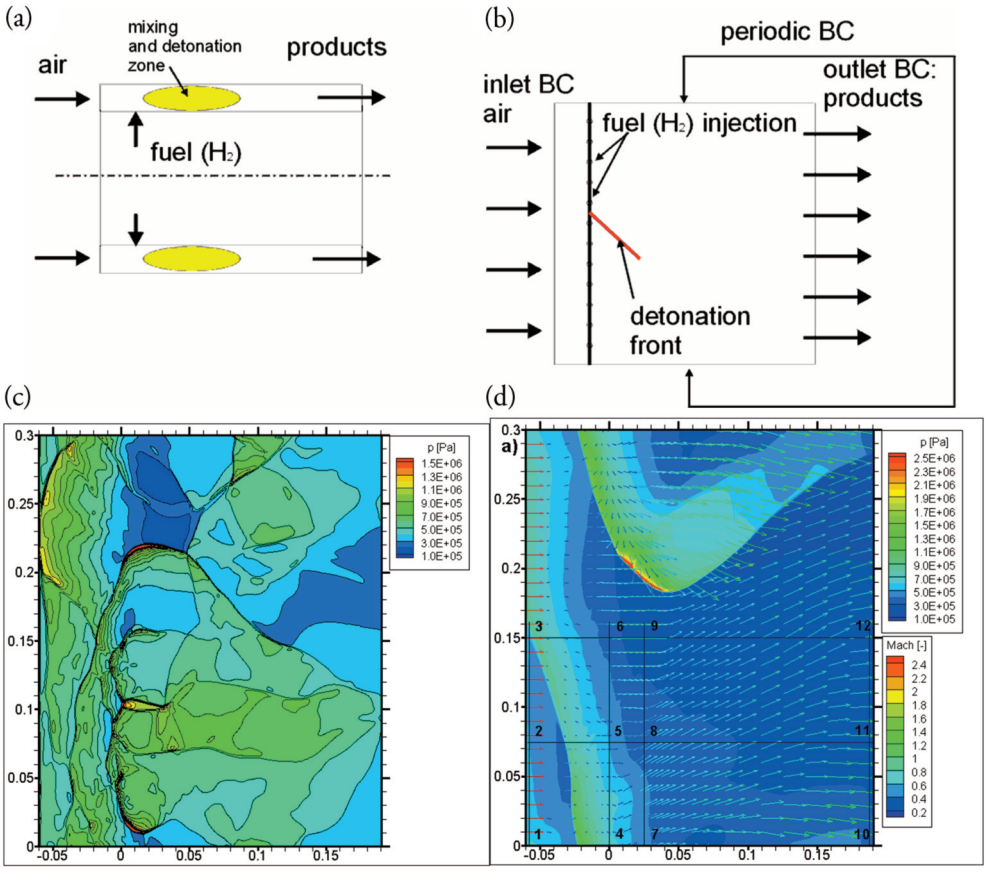

Fig. 15. (a,b) Chamber geometry; (c) contours of unstable detonation after ignition; (d) single detonation wave stabilizes after some time [39].

If the initial rotating detonation wave is successfully generated, it either stabilizes or multiple detonation fronts are generated or detonation extinguishes, depending on the fresh mixture feeding rate (see Wave Number theory of Wolanski in [40]). The presented methodology does not influence the ultimate result, but it speeds up its receipt by avoiding the creation of two detonation waves propagating in opposite directions during the ignition. Two examples of (a) successful and (b) unsuccessful initiation of rotating detonation is shown in Figure 16.

During the detonation initiation considerable time is needed to reach the stable regime. Therefore, it is of advantage to use previous solutions to initialize the new computational case whenever possible.

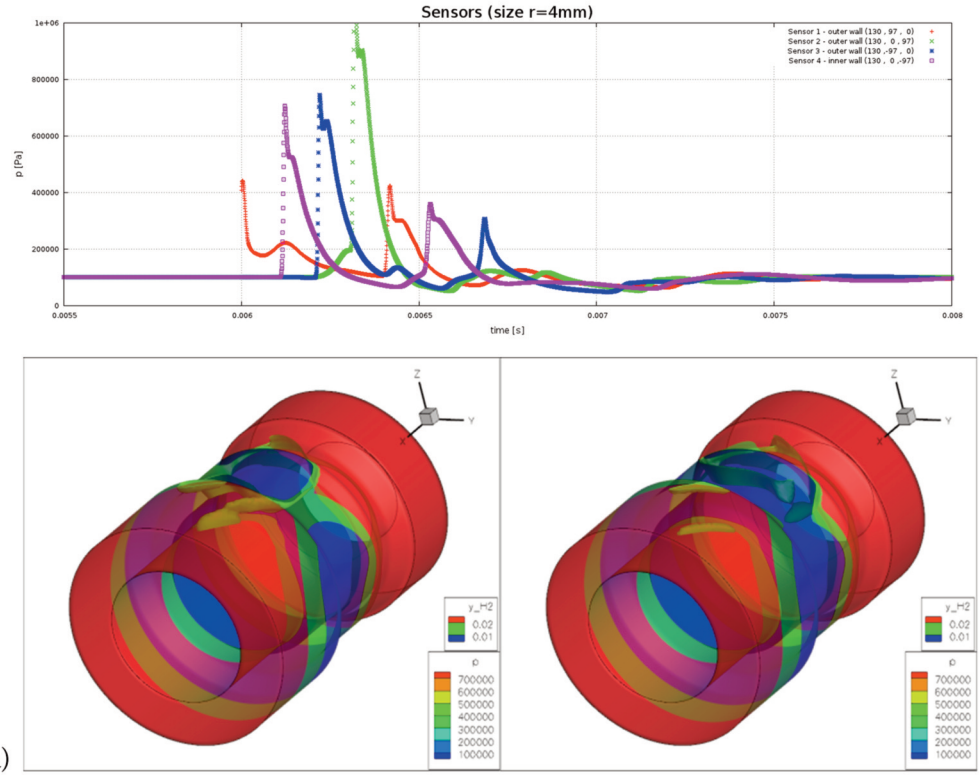

(a)

Fig. 16. Pressure sensor readings, and 2 selected contour plots of hydrogen mass fraction and pressure isosurfaces of (a) unsuccessful initiation of numerical rotating detonation in combustion chamber of the RDE. The main flow direction is along X axis.

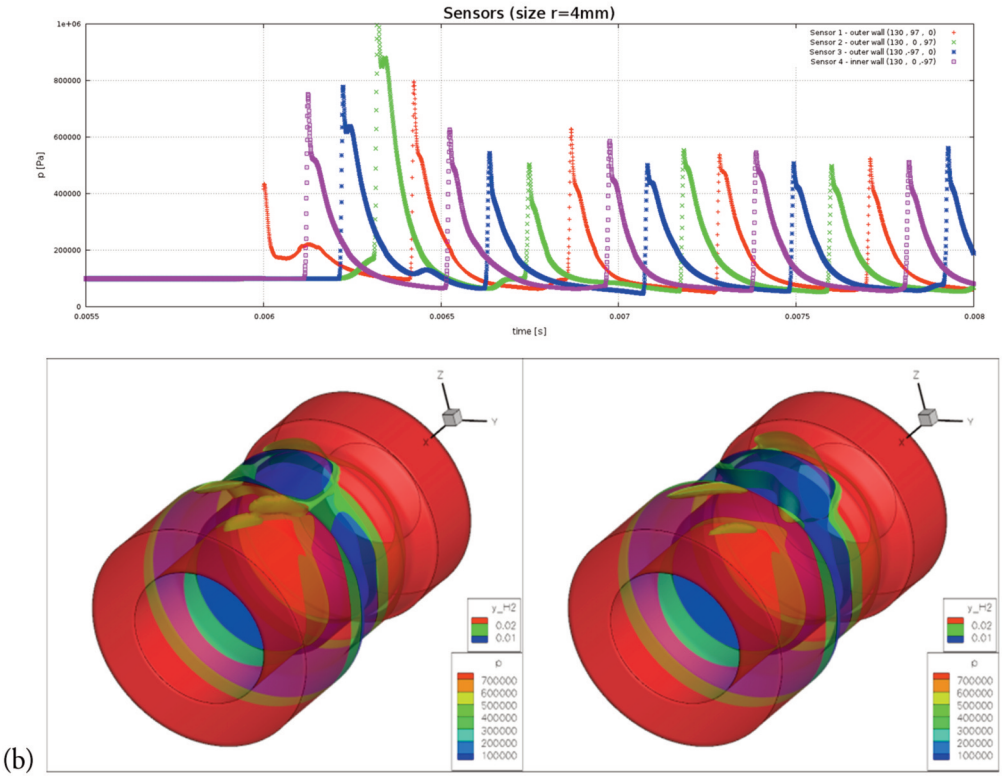

(b)

Fig. 16. Pressure sensor readings, and 2 selected contour plots of hydrogen mass fraction and pressure isosurfaces of (b) successful initiation of numerical rotating detonation in combustion chamber of the RDE. The main flow direction is along X axis.

5.2. Stepped combustion chamber

In the following section the analysis of results of simulations of the stepped combustion chamber of the Rotating Detonation Engine investigated at Institute of Aviation in Warsaw is presented. Different inlet parameters, viscous and inviscid gas models, premixed gas or with use of numerical injectors are compared with each other and with experimental results. Additionally, the measured performance and accuracy of implementation of Adaptive Mesh Refinement method is presented and further recommendations are drawn.

Case description

The stepped combustion chamber consists of two annular sections of heights 22 and 50 millimetres (see Figure 17). The injection of gaseous hydrogen is realized with 90 orifices of 0.7 mm diameter, placed perpendicularly to the flow direction at the inner surface of throat. In the considered case pressure sensor is placed at the outer surface, in the middle of the first section.

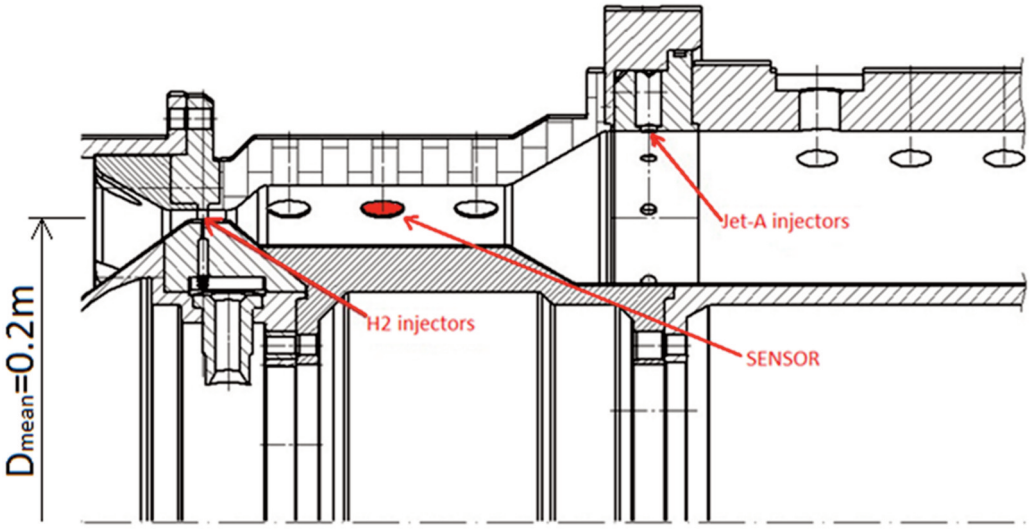

Fig. 17. Geometry of the stepped combustion chamber of the RDE. The main flow direction is from left to right.

The computational model of the stepped chamber was build up from 190 000 hexahedral elements (see Figure 18), the smallest element size is 2.2 mm. Numerical sensors and injectors (in case of non-premixed calculations) are placed at positions corresponding to positions of real devices.

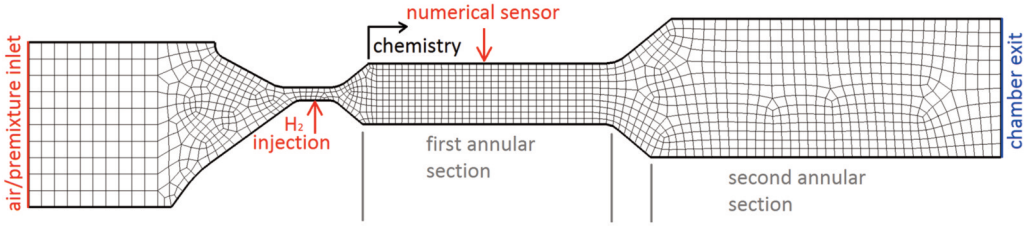

Fig. 18. Longitudinal section of computational model of the RDE stepped geometry.

In case of premixed computations and when no mixing model is used, it is of advantage to suppress chemical source terms in detonation simulations in certain subdomains of computational model. Such manipulation can be used to imitate the mixing length. In Figure 18 it is shown that in presented case the chemical reaction can occur only downstream the first divergent section.

Computations of detonation in premixed gas

Twelve inviscid, premixed simulations have been performed for various supersonic inlet conditions and mixture compositions:

- air-fuel equivalence ratio λ =1 (stoichiometry), λ =1.5 and λ =2 (lean mixtures);
- inlet pressure p_{in}= 2, 3, 4 or 6 bar;
- isentropic compression from standard conditions was assumed at inlet, inlet temperature set to T_{in}= 357.4, 401.2, 435.6 or 489.1 K for respective inlet pressures.

For all cases standard outlet conditions (T_{out} =293.15 K, p_{out} =1.01325 bar) were assumed. Details of the implementation of boundary conditions in REFLOPS USG are provided in PhD thesis of Swiderski [23].

The resulting mean outlet parameters are presented in Table 1. Several conclusions drawn on the basis of presented data are listed below.

- Mean outlet pressure is higher than the prescribed boundary conditions, the difference is the higher the higher the inlet pressure is. It proves that there exists region of supersonic flow at outlet. The raised mean outlet pressure is caused by oblique shock wave, entailed by the detonation wave, which extends downstream to the outlet section.
- The mean flow velocity at outlet is subsonic in each case. The velocity is the higher, the higher the inlet pressure is, and similar for various air-fuel equivalence ratios.
- Mean axial velocity and mean velocity magnitude at outlet differ by less than 5%. On the basis of the above data it may be said the flow is axial.
- The obvious result is that higher mass flow rate is obtained for higher inlet pressure. However, outlet pressure is slightly less for higher air-fuel equivalence ratios and the outlet density raises. This causes the mass flow rate to rise slightly as the amount of fuel in the premixture is decreased.
- There is quite a high residue of H2 in exit section. It is shown that less than 8% of fuel remains unreacted in case of high pressures and about 3% for low pressure rations.

Tab. 1 Mean flow parameters at the outlet of combustion chamber (static, and total pressure, density, temperature, axial velocity, velocity magnitude, hydrogen mass fraction and mass flow rate) for various inlet conditions.

Case	p [bar]	p_{total} [bar]	ρ [kg/m3]	T [K]	u [m/s]	V [m/s]	y_{H_2} [-]	$\dot{m}$ [kg/s]
$p_{in} = 2\ bar, \lambda = 1$ *								
$p_{in} = 3\ bar, \lambda = 1$	1.22	1.25	0.25	1540	146	150	0.13%	1.02
$p_{in} = 4\ bar, \lambda = 1$	1.25	1.32	0.22	1771	227	234	0.16%	1.48
$p_{in} = 6\ bar, \lambda = 1$ **	1.82**	2.14**	0.23**	2320**	499**	511**	0.24%**	3.65**
$p_{in} = 2\ bar, \lambda = 1.5$ *								
$p_{in} = 3\ bar, \lambda = 1.5$	1.19	1.22	0.29	1341	136	141	0.05%	1.14
$p_{in} = 4\ bar, \lambda = 1.5$	1.24	1.30	0.27	1481	201	207	0.06%	1.61
$p_{in} = 6\ bar, \lambda = 1.5$	1.29	1.45	0.22	1801	353	366	0.10%	2.44
$p_{in} = 2\ bar, \lambda = 2$	1.15	1.16	0.42	925	68	70	0.03%	0.79
$p_{in} = 3\ bar, \lambda = 2$	1.17	1.20	0.32	1209	133	138	0.05%	1.25
$p_{in} = 4\ bar, \lambda = 2$	1.19	1.26	0.26	1476	220	225	0.08%	1.74
$p_{in} = 6\ bar, \lambda = 2$	1.25	1.40	0.24	1638	333	348	0.11%	2.53

* detonation decays
** unstable case

Pressure sensor readings are presented in Figures 19, 20 and 21. Note that in cases of inlet pressure p_{in}=2 stable detonation wave was obtained for long term only in case p_{in}= 2 bar, λ =2. In other two cases the instabilities started to arise in time and detonation decayed the faster the lower the air-fuel equivalence ratio became (not shown). The inflow velocity is constant in each case for constant inlet pressure p_{in}= 2 bar, while the C-J speed that characterizes detonation wave velocity is the higher, the lower the air-fuel equivalence ratio is. Therefore, it can be concluded that the decay of detonation is due to too low flow rate (and velocity) of fresh mixture relative to the circumferential velocity of detonation wave.

Pressure peaks in the remaining cases are very regular and single stable detonation wave is observed (except for one). Surprisingly, the highest pressure peaks are obtained for inlet pressure p_{in}= 4 bar, slightly lower for p_{in}= 6 bar and much lower for p_{in}= 3 bar. The same regularity holds true for speed of detonation wave (see Table 2) The highest pressure peaks and detonation speed are reported for high inlet pressure

and stoichiometric mixture (p_{peak} = 7.6 bar, V_{DET} =1716 m/s). The lowest peaks are observed for lean mixture λ = 2 and low inlet pressure p_{in}= 2 bar (p_{peak} = 4 bar, V_{DET} =1092 m/s).

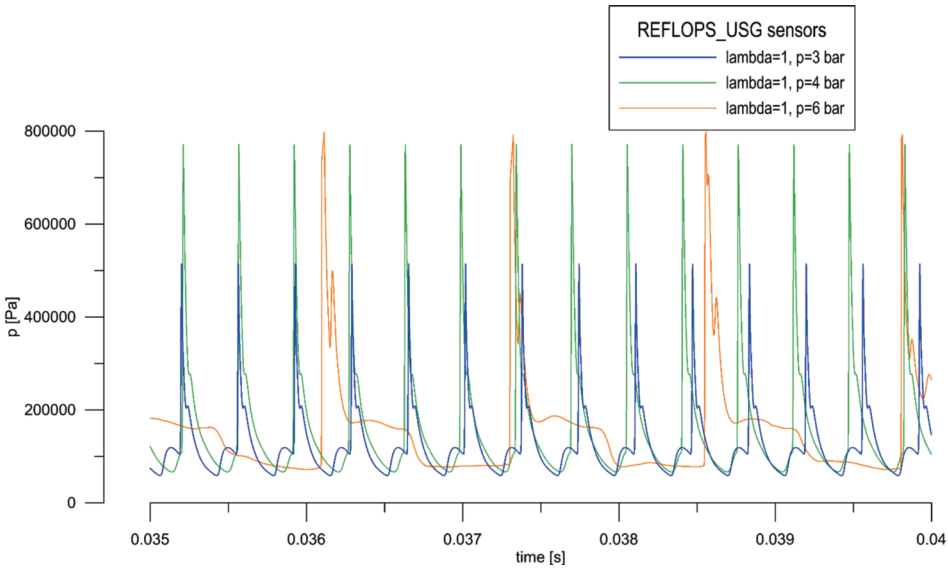

Fig. 19. Pressure sensor plot for λ = 1 and various inlet pressures.

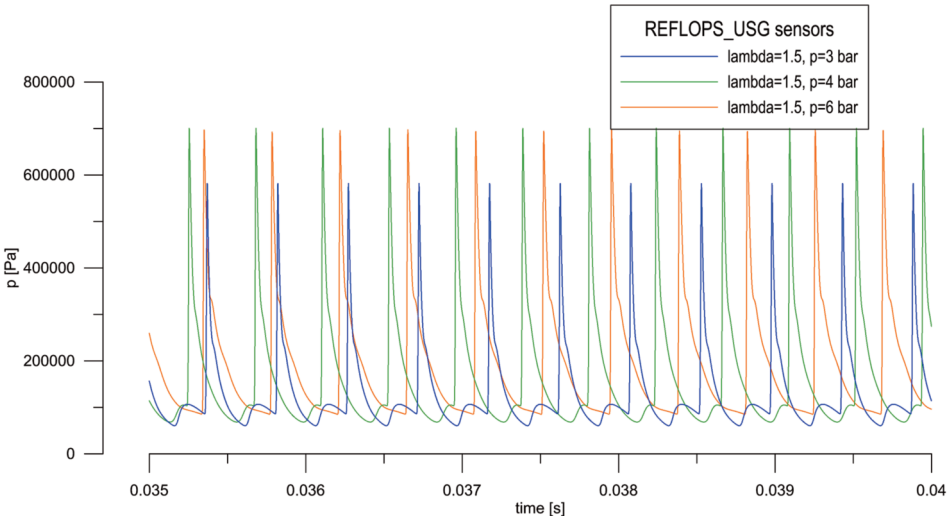

Fig. 20. Pressure sensor plot for λ = 1.5 and various inlet pressures.

The Chapman-Jouguet detonation velocity for initial pressure in range 1 to 6 bar is for considered mixtures of λ =1, λ =1.5 and λ =2 in range 1967-2001 m/s, 1758-1768 m/s and 1608-1610 m/s respectively. The measured detonation velocity shown in Table 2 is about 15% (300 m/s) lower for stoichiometric mixtures and 25% (400 m/s) lower for lean mixtures. These discrepancies can be justified by relatively coarse mesh (minimum cell size 2.2 mm) which was a compromise between an acceptable accuracy and performance required during the preliminary design process. It will be further shown that when finer mesh is used, results much closer to theoretical values are obtained.

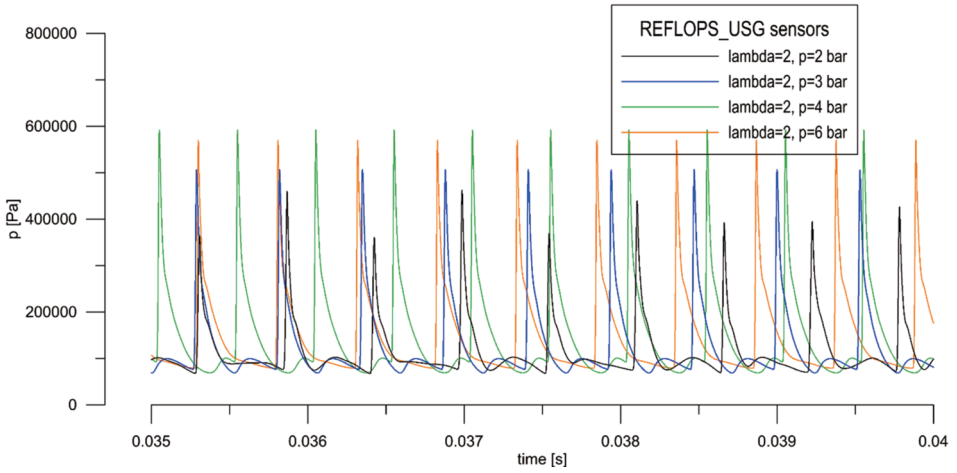

Fig. 21. Pressure sensor plot for $\lambda = 2$ and various inlet pressures.

Tab. 2. Frequency and detonation wave speed (calculated for the mean circumference 0.635m) for various inlet conditions.

Case	frequency [kHz]	wave speed [m/s]	p_{peak} [bar]
$p_{in} = 2\ bar, \lambda = 1.0$*			
$p_{in} = 3\ bar, \lambda = 1.0$	2.75	1679	4.9
$p_{in} = 4\ bar, \lambda = 1.0$	2.81	1716	7.6
$p_{in} = 6\ bar, \lambda = 1.0$**	0.79	N/A	9.5
$p_{in} = 2\ bar, \lambda = 1.5$*			
$p_{in} = 3\ bar, \lambda = 1.5$	2.22	1352	5.7
$p_{in} = 4\ bar, \lambda = 1.5$	2.34	1429	6.9
$p_{in} = 6\ bar, \lambda = 1.5$	2.30	1405	6.85
$p_{in} = 2\ bar, \lambda = 2.0$	1.79	1092	4
$p_{in} = 3\ bar, \lambda = 2.0$	1.88	1150	5
$p_{in} = 4\ bar, \lambda = 2.0$	1.99	1216	5.8
$p_{in} = 6\ bar, \lambda = 2.0$	1.96	1197	5.6
* unstable case ** detonation terminates			

The very different situation occurred in case p_{in}= 6 bar, λ =1 where sequence of pressure peaks of much lower frequency is observed (see Table 2). The detailed analysis of this case revealed the very regular sequence of explosions (see Figure 22) similar to the work cycle of Pulse Detonation Engine (there is no shutter in this case, but the flow is choked which may cause similar effect). The observed cycle can be subdivided as follows:

- the chamber is refilling with fresh mixture for about 1 000 microseconds;
- the ignition occurs as soon as fresh mixture reaches the higher section of combustion chamber, where the recirculation region of hot products is attached;
- the detonation terminates after 200 microseconds and the cycle repeats.

The described process has not been observed in experiment to date, since no experiment has been conducted for similar inlet conditions. On the other hand, the modeling of initiation of detonation plays an important role in the observed process. Therefore, the occurrence of 'pulsed' mode in the chamber of the Rotating Detonation Engine should be confirmed by more detailed simulations or validated experimentally.

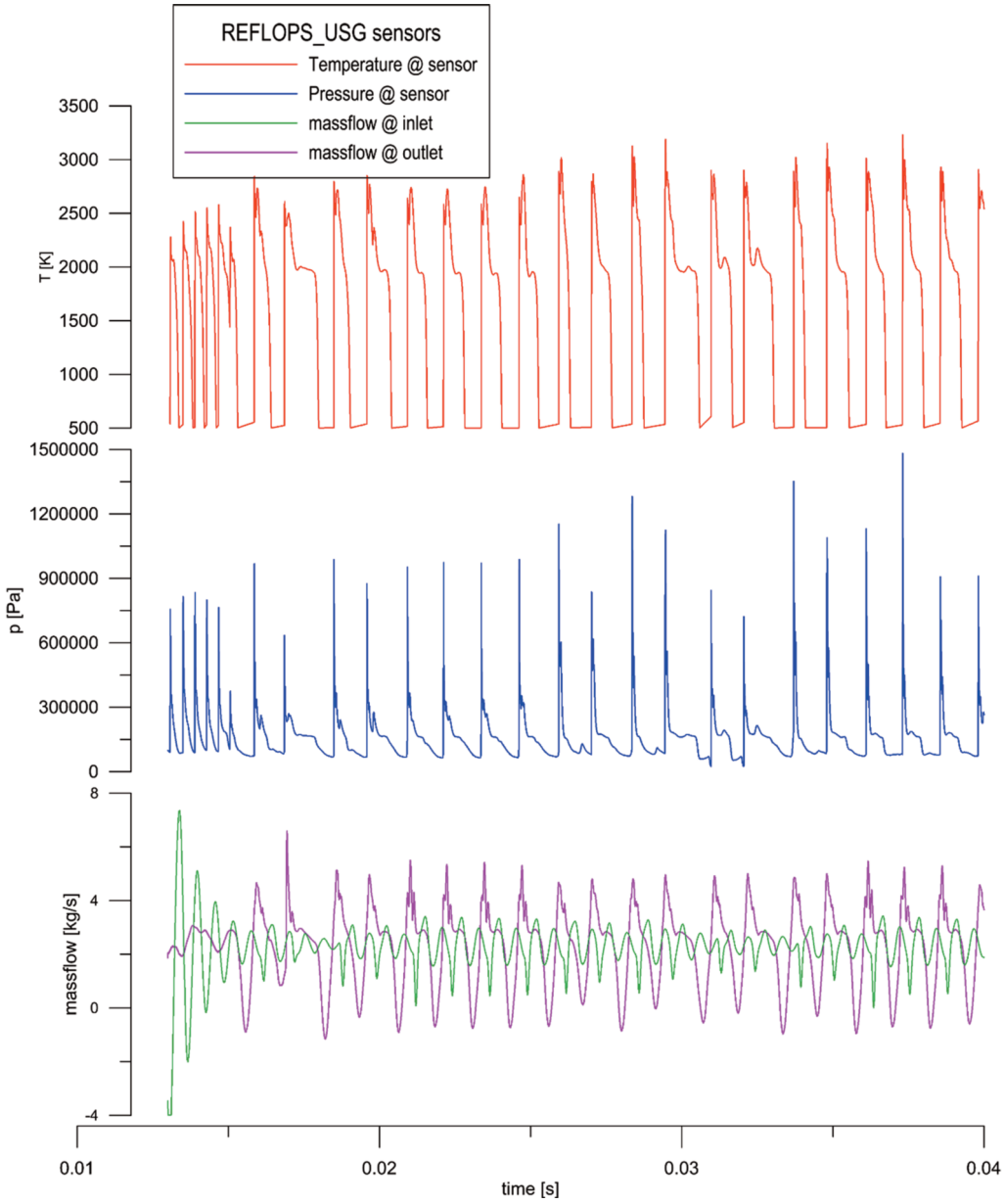

Fig. 22. Pressure and temperature peaks at sensor and mass flow rate at inlet and outlet in case p_{in}= 6 bar, λ =1.

Comparison with experimental results

The assessment of three approaches to modeling of combustion chamber of RDE was performed. The study has been conducted on:

- simple model of inviscid flow with homogenous gas mixture investigated earlier;

and two more sophisticated and computationally expensive models, namely:

- model of inviscid flow with numerical injection of hydrogen;
- model of viscous flow with numerical injectors and the standard k-e turbulence model.

The detailed description of viscosity and two-equation turbulence models in REFLOPS USG can be found in PhD thesis of Swiderski [9].

Simulations have been performed for input conditions adapted from experiment, namely:

- inlet air pressure: 4.2 bar;
- inlet air temperature: 390 K;
- mass flow rate of hydrogen: 28.4 g/s;
- resulting mass flow rate of air: 2.001.

The reading from the pressure sensor registered in this experiment is presented in Figure 23. The pressure peaks are mostly in the range of 4-6 bar. However, there are also stronger peaks observed, up to 10-12bar.

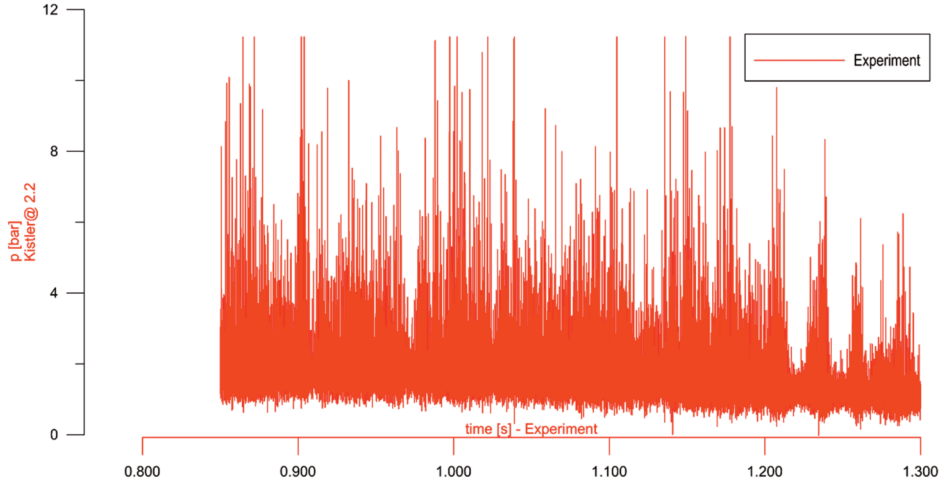

Fig. 23. Pressure sensor reading from experiment.

The most representative experimental results were selected and compared with 3 modeling approaches. Comparison of pressure sensor readings is shown in Figure 24. It can be observed that the resulting working frequency in each simulation is very similar and agrees qualitatively with measured during experimental research.

Exact measurements of detonation wave speed are shown in Table 3. It is important to note, that the linear wave speed measured along the mean circumference almost exactly matches the C-J velocity, which is 1609 m/s in this case. Pressure peaks are higher than in experiment in case of inviscid and viscous injection, and even higher in case of premixed gas.

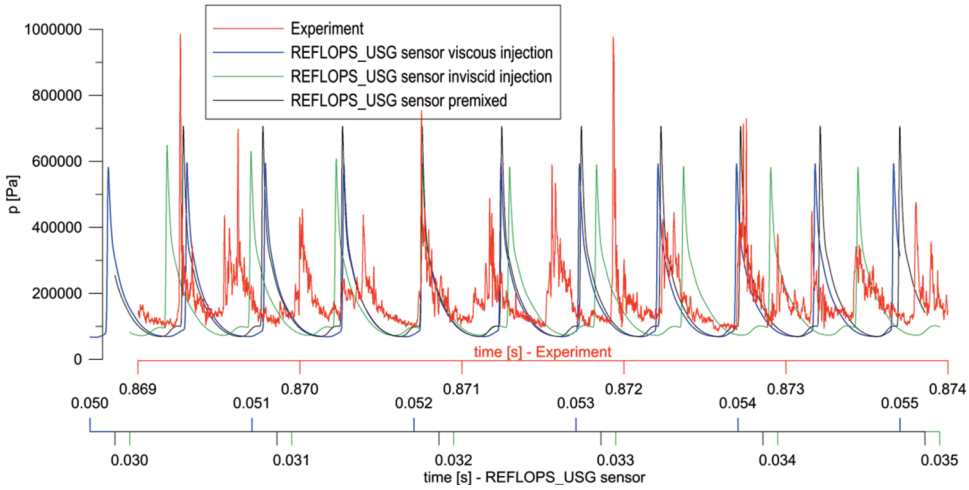

Fig. 24. Comparison of pressure profiles at sensors.

Tab. 3. Comparison of detonation parameters for case p_{in}= 4.2 bar, λ =2.

Case	λ	Temperature at outlet [K]	Wave speed [m/s]	Mean pressure peak p_{peak} [bar]	Specific impulse ISP_f [s]
Experiment	2.05	1198	1605	5	N/A
Simulation, viscous, injection	2.13	1450	1258	6	4040
Simulation, inviscid, injection	2.08	1341	1143	6	4550
Simulation, premixed, denoted $p_{in} = 4.2\ bar, \lambda = 2$	2.00	1345	1243	7	4670

Thrust $\boldsymbol{F}$ and fuel-based specific impulse ISP_f are evaluated according to the following equations:

$$F = \int \left(\rho u^2 + p - p_\infty\right) dA \qquad ISP_f = \frac{F}{g\dot{m}_f}, \tag{13}$$

where ρu^2 and p are normal momentum and pressure at chamber exit, p_∞ is ambient pressure, g and $\dot{m}_f$ are gravity acceleration and fuel mass flow rate respectively. Results of specific impulse measurements are very promising and in case of inviscid computations shown in Table 3 are all in range 4550-4750 s. In case of RANS simulations the value of specific impulse is considerably reduced by viscous losses.

It is important to note, that the experimental temperature at outlet listed in Table 3 is not measured directly. The overall time of experiment was too short for thermocouple to reach the equilibrium temperature. However, it was found that the approximation of the transmittance of thermocouple with a second-order inertial term gives good results. The least squares fit is used to extrapolate the results .

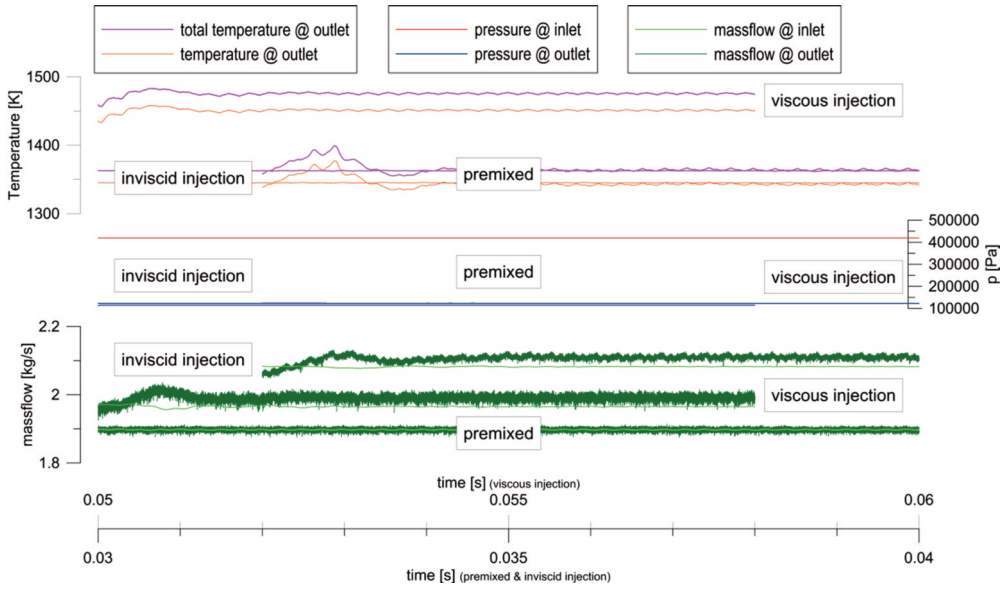

Fig. 25. Comparison of parameters at inlet and outlet sections.

Representative parameters selected for Table 3, presented in Figure 25 and pressure isosurfaces shown in and Figure 26 prove that differences in results between models are relatively small, when comparing with experimental results. These differences are of minor importance, especially at the stage of preliminary design of the RDE chamber, when usually only qualitative agreement between experimental and numerical results is expected.

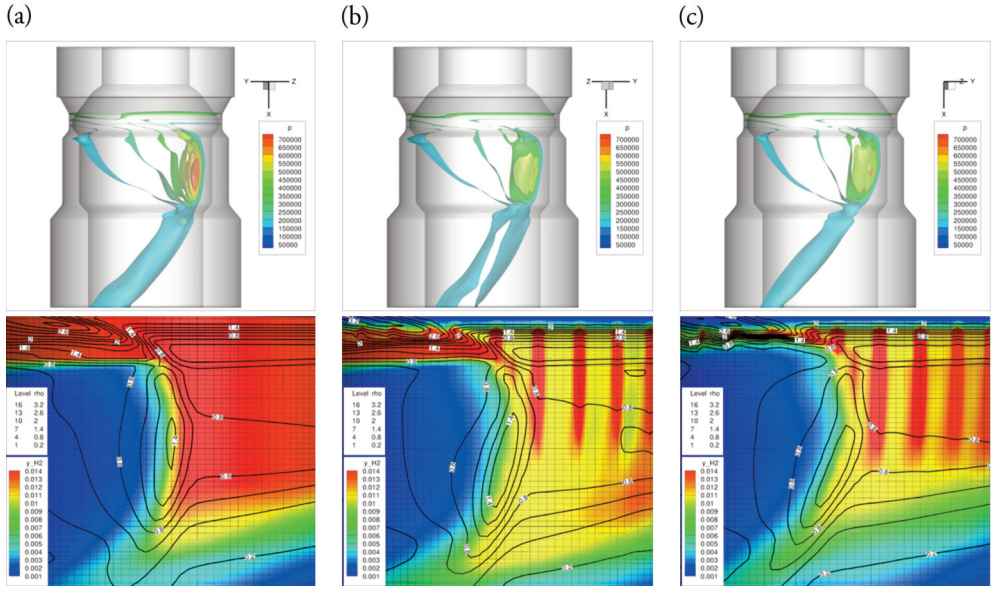

Fig. 26. Isosurfaces of static pressure, isolines of density and contours of mass fraction of hydrogen. Results of simulations: (a) inviscid and premixed, (b) inviscid and (c) viscous with hydrogen injection. The main flow direction is from up to bottom.

Flow field structure analysis

The research presented here is intended to show the qualitative agreement of the selected numerical model with experimental results. Although the detailed structure of rotating detonation is beyond the scope of the presented research, the model and grid resolution used offer satisfactory accuracy to resolve the general flow field structure and the pattern of waves associated with the rotating detonation front. Some interesting features of rotating detonation in this geometry will be highlighted below. The case selected for analysis is p_{in}= 4.2 bar, λ =2 investigated in the previous subsection.

In Figure 27 contours of static pressure, temperature and hydrogen mass fraction are plotted in selected sections. It is shown that the region of highest pressure is located in the half-length of low section of combustion chamber. The region of highest temperature is located at the very beginning of the low section of the chamber, just after the divergent nozzle. Both the pressure and the temperature are not equally distributed radially. The highest pressure and temperature regions are located at the outer surface of combustion chamber.

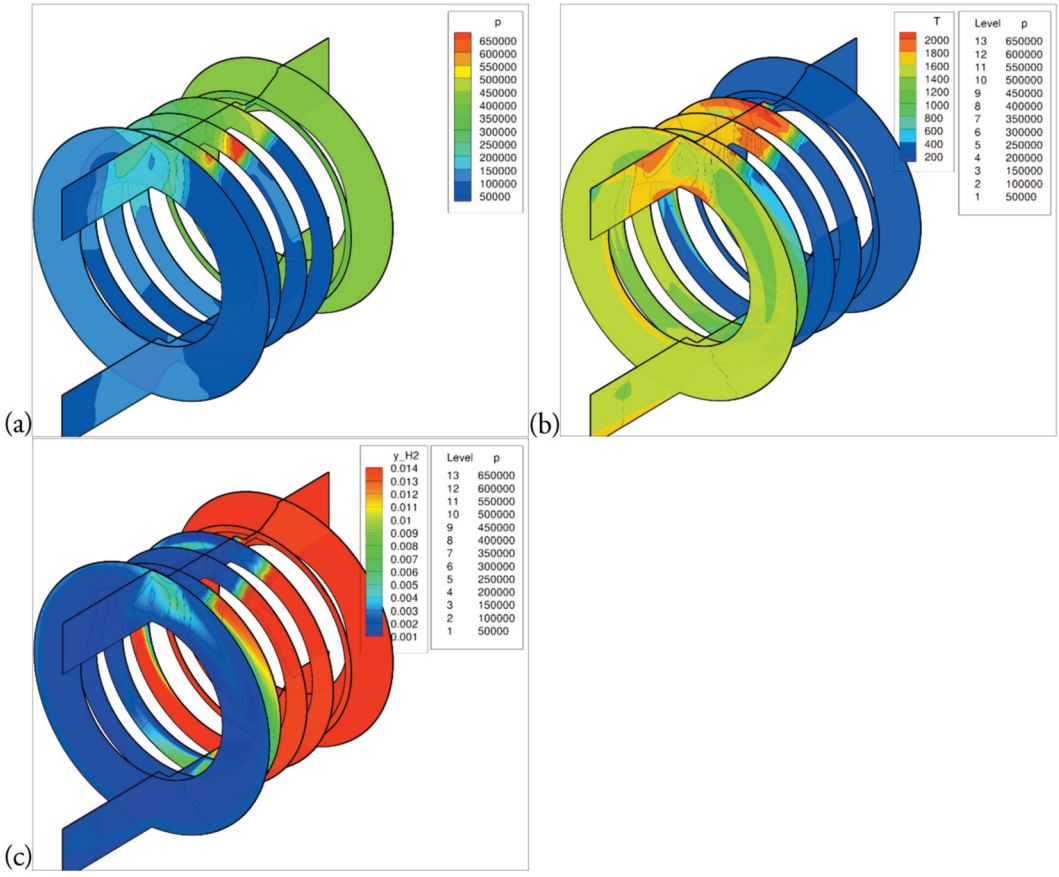

Fig. 27. Contours of (a) pressure, (b) temperature, (c) mass fraction of hydrogen and isolines of pressure in selected sections of combustion chamber.

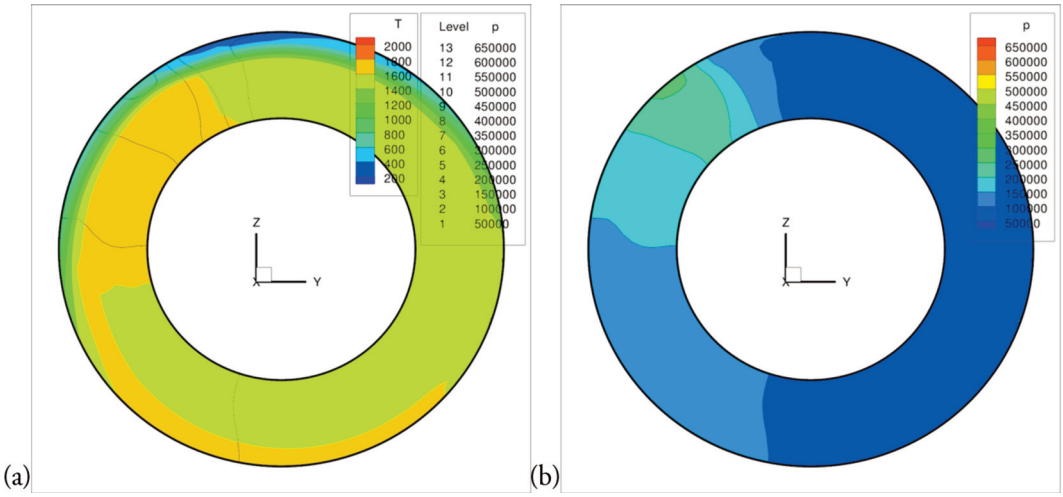

Fig. 28. (a) Temperature and (b) pressure distribution at outlet section.

In Figure 28 contour maps of outlet parameters are shown. It is again conformed that the detonation wave reaches the outlet of combustion chamber, and the relatively high pressure occurs at the outer surface of combustion chamber. The temperature is distributed more uniformly.

In Figure 29 the axial and non-axial components of velocity are shown. In (c) it is shown that the circumferential velocity component dominates the non-axial velocity, and radial component is relatively small. The highest axial velocity of 500 m/s is observed in the middle of channel height. The following conclusions can be drawn.

- The flow far from the detonation wave is nearly axial.
- The flow before the detonation wave is the more circumferential the closer the wave is. The maximum axial velocity is about 200 m/s.
- The axial velocity before the detonation wave is relatively small (about 200 m/s in the middle of channel height). Backflow of velocity not greater than 50 m/s is observed at the outer surface.
- The non-axial velocity on the other side of the wave is opposite. Both the axial and non-axial velocities are the highest in the middle of the height of combustion chamber, at the detonation front.
- The axial velocity stays high for half of the chamber circumference and dominates the flow, since the non-axial component vanishes at a distance of 45 degrees from the detonation front.

The mean axial velocity and mean velocity magnitude at outlet differ by less than 5%. The instantaneous results shown in this section are not of practical importance in terms of performance. Since the working frequency of the RDE is of order of several kHz, it may be said that the flow is nearly axial. However, the presence of high velocity gradients and shock wave at outlet section must be kept in mind.

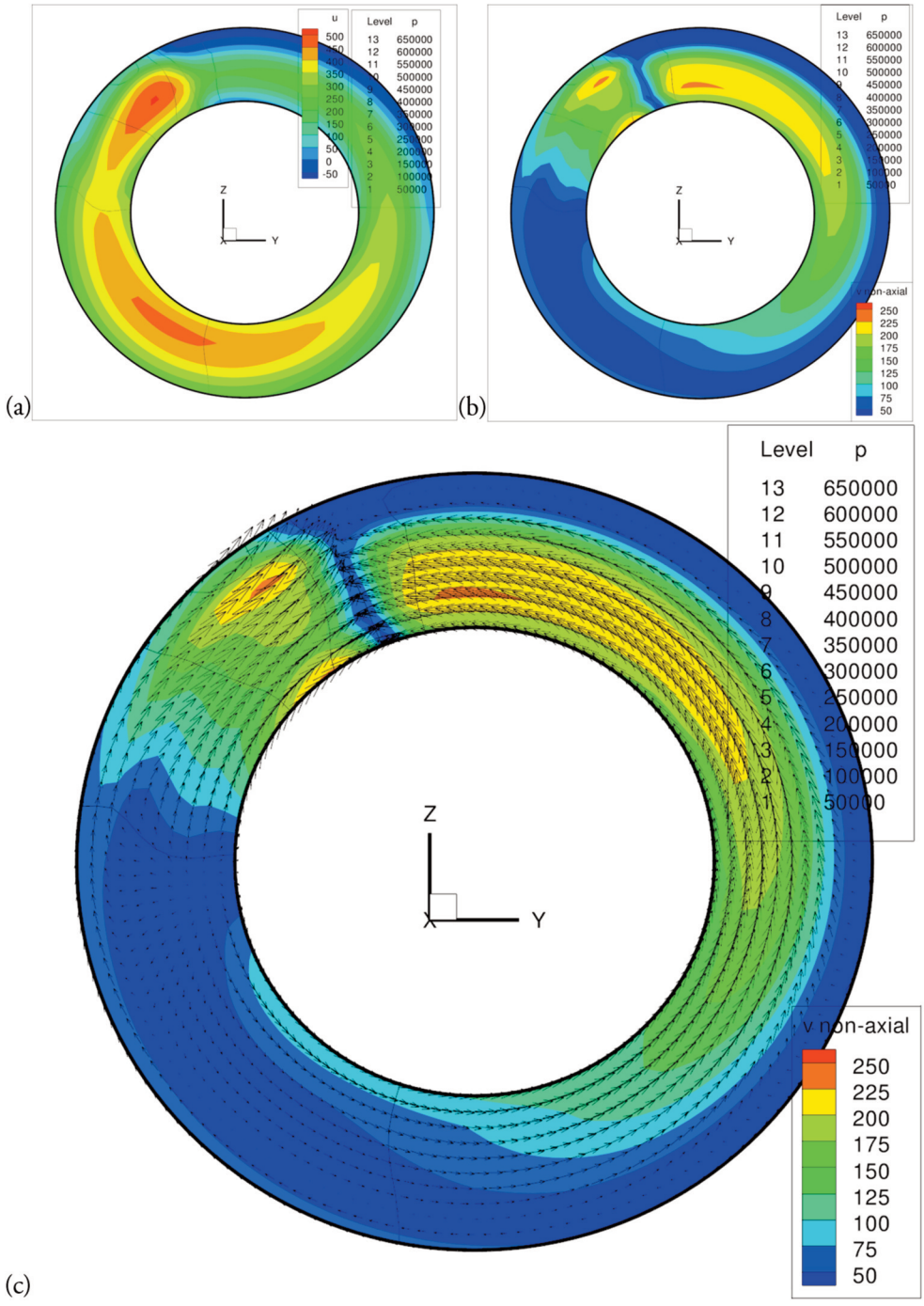

Fig. 29. (a) Axial and (b) non-axial velocity distribution at outlet section.
(c) Non-axial velocity vectors and magnitude of non-axial velocity.

Second-order scheme

All results presented in previous subsections were obtained with use of first-order HLLC solver. Below, comparison of results of first and second-order schemes is presented.

In Figure 30 comparison of pressure sensor readings is shown. It can be observed that for second-order scheme the resulting working frequency is closer to experimental result. Pressure peaks obtained in inviscid numerical simulations are higher than experimental. This is due to the lack of diffusive terms in governing equations. For higher-order schemes also the artificial diffusion introduced by numerical methods is lower and pressure peaks are even higher. In Figure 31 the flow field near the detonation front obtained with use of two schemes is shown. Isolines of density indicate location of waves, which are noticeably sharper in case of second-order scheme. Further study on the influence of limiters on results can be found in [34].

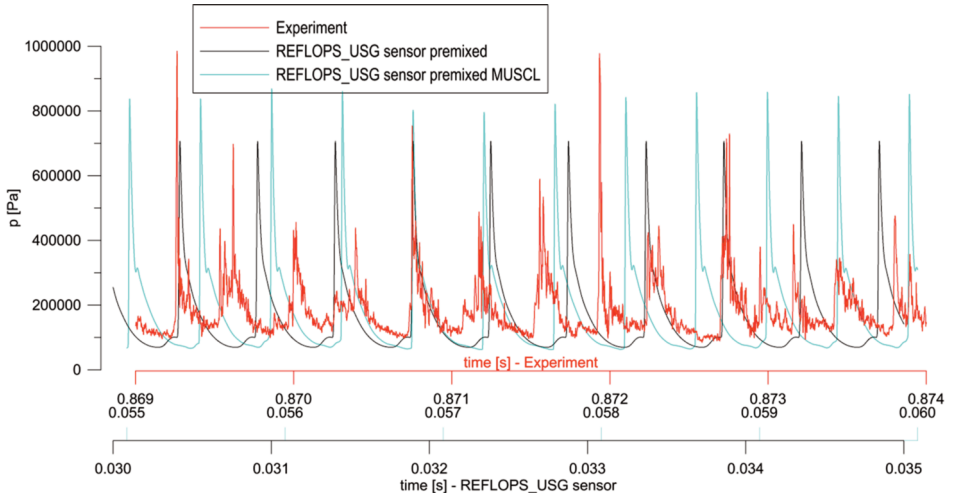

Fig. 30. Comparison of pressure profiles at sensors.

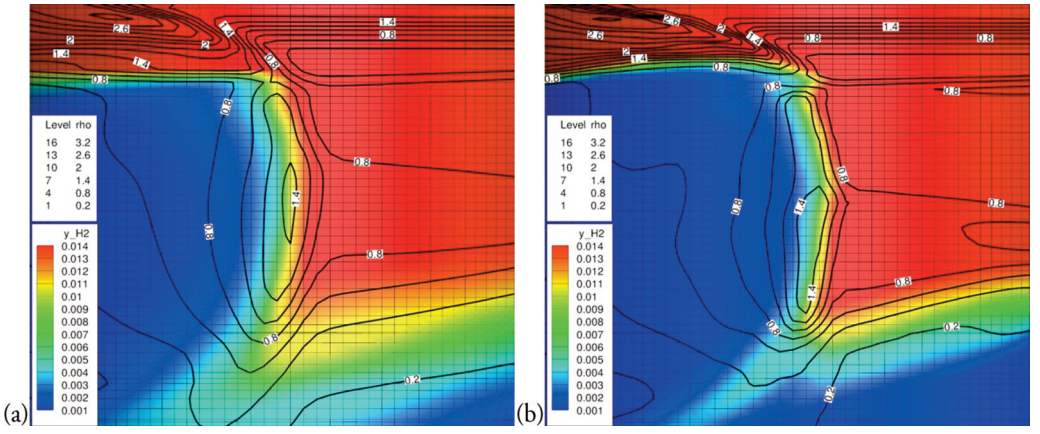

Fig. 31. Isolines of density and contours of mass fraction of hydrogen. Results of simulations (a) 1st-order HLLC (b) 2nd-order MUSCL-Hancock HLLC. The main flow direction is from up to bottom.

Performance of AMR

The detailed research on the AMR refinement criterions was performed for the two two-dimensional tests of shock and detonation wave wedge reflection in . Similar, such detailed comparison can be hardly reproduced for the three-dimensional rotating detonation wave simulations due to the memory limitations. The selected method of quantitative accuracy comparison requires reference solution for error measurements. The memory requirement for any useful reference solution in this case (3D mesh, at least fully refined to 3rd AMR level) is $(2^3)^3 = 512$ greater than for the base grid. Therefore, only qualitative comparison will be done in this case for refinement criterion selected during previous tests. The most representative results of this comparison, obtained on (a) coarse mesh and (b) grid fully refined to 2nd AMR level are shown in Figure 32 and 33.

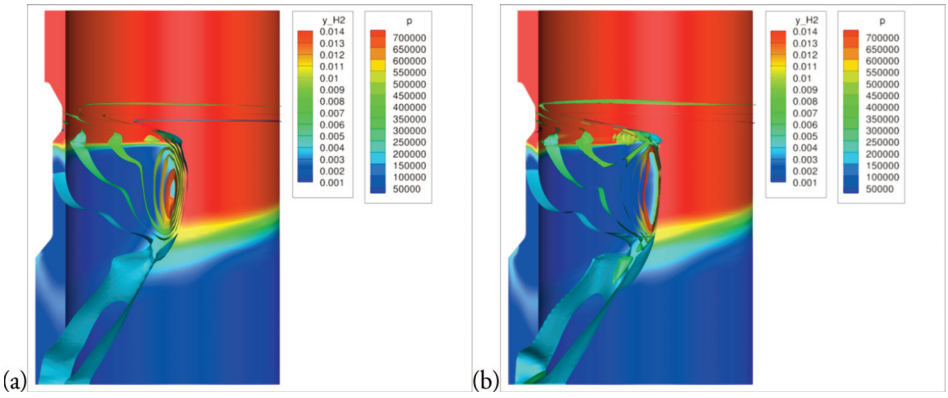

Fig. 32. Isosurfaces of pressure and contours of mass concentration of hydrogen plotted at the cylindrical surface of mean chamber height in case: (a) base grid, no AMR; (b) fine grid, fully refined to 2nd AMR level.

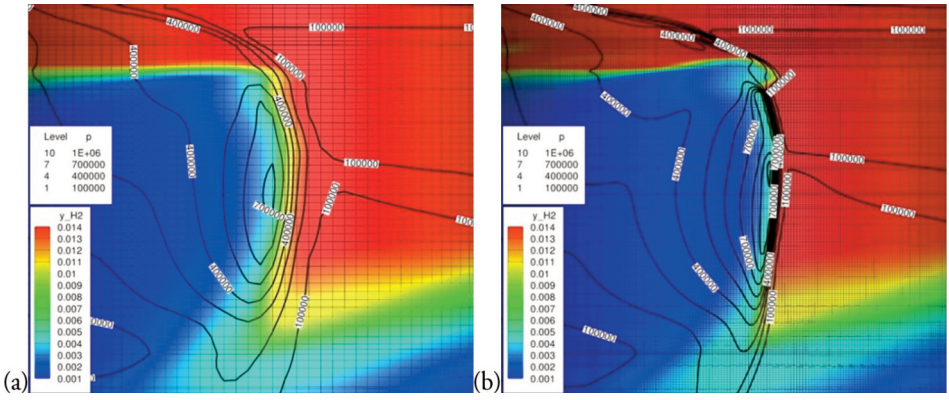

Fig. 33. Isolines of pressure and contours of mass concentration of hydrogen near detonation front in case: (a) base grid, no AMR; (b) fine grid, fully refined to 2nd AMR level.

Measurement of execution time of the code has been performed for cases running for 50 microseconds with different values of refinement threshold and 1 or 2 maximum levels of refinement allowed. Results of these measurements are shown in Table 4 and Figure 34 (b).

Tab. 4. Overall wall time for various thresholds of density gradient based refinement criterion.

	Overall wall time of execution [s]	
ε_R [-]	AMR1	AMR2
AMR0 (base grid)	**138**	**138**
2	216	686
0.2	391	4864
0.02	**1059**	**15832**
0.002	2353	40897
0.0002	2725	48023
FULL (fully refined)	**2711**	**48023**

Comparison of pressure sensor readings for cases running for 900 microseconds is shown in Figure 34 (d).

On the basis of obtained results, several conclusions have been drawn:

- solution obtained for $\varepsilon_R = 0.0002$ is indistinguishable from solution on fully refined grid, since the grid is almost fully refined;
- solution obtained for $\varepsilon_R = 0.002$ is almost identical to solution on fully refined grid, while it is slightly faster (compare red line and dashed blue line in Figure 34 (d));
- solution obtained for $\varepsilon_R = 0.02$ is almost identical to solution on fully refined grid, while it is 2.5 to 3 times faster (compare red line and dashed orange line in Figure 34 (d));
- solution obtained for $\varepsilon_R = 0.2$ is 7 to 10 times faster than solution obtained on base grid. Unfortunately, the agreement of result is unacceptable (compare red line and dashed light green line in Figure 34 (d));
- solution obtained for $\varepsilon_R = 2$ is of unacceptable accuracy and comparable to base grid solution.

Results of previous tests have shown that criterions based on density gradient give the best results. It is shown above, that in case of simulations of the Rotating Detonation Engine, the threshold values of density gradient based criterion should be of order of 0.02 and lower.

Despite the arising discrepancy in threshold values, there is also similarity that can be observed. The speedup achieved for properly selected threshold should be from 2 for single level, through 3 in case of 2 levels, to 4 in case of 3 levels of refinement allowed. Much greater speedup, relative to fully refined grid is hardly possible without severe degradation of solution accuracy.

Similar conclusion had been drawn by Eude and Davidenko in for the RDE chamber simulations on structured grids. They reported runtime reduction by a factor of more than 2 for two AMR levels allowed. They emphasized that in spite of an important memory saving as the total number of computational cells is lesser by 60% with AMR, the runtime cannot be reduced to the same ratio as the number of cells. This is due to the significant computational overhead of the AMR algorithm.

The recommendation for the one who wants to select an appropriate threshold of refinement criterion for simulation of the Rotating Detonation Engine is to base the initial estimate on speedup criterion proposed above. No certain threshold value can be suggested here. The selected threshold can be further verified through simple qualitative analysis demonstrated in Figure 34.

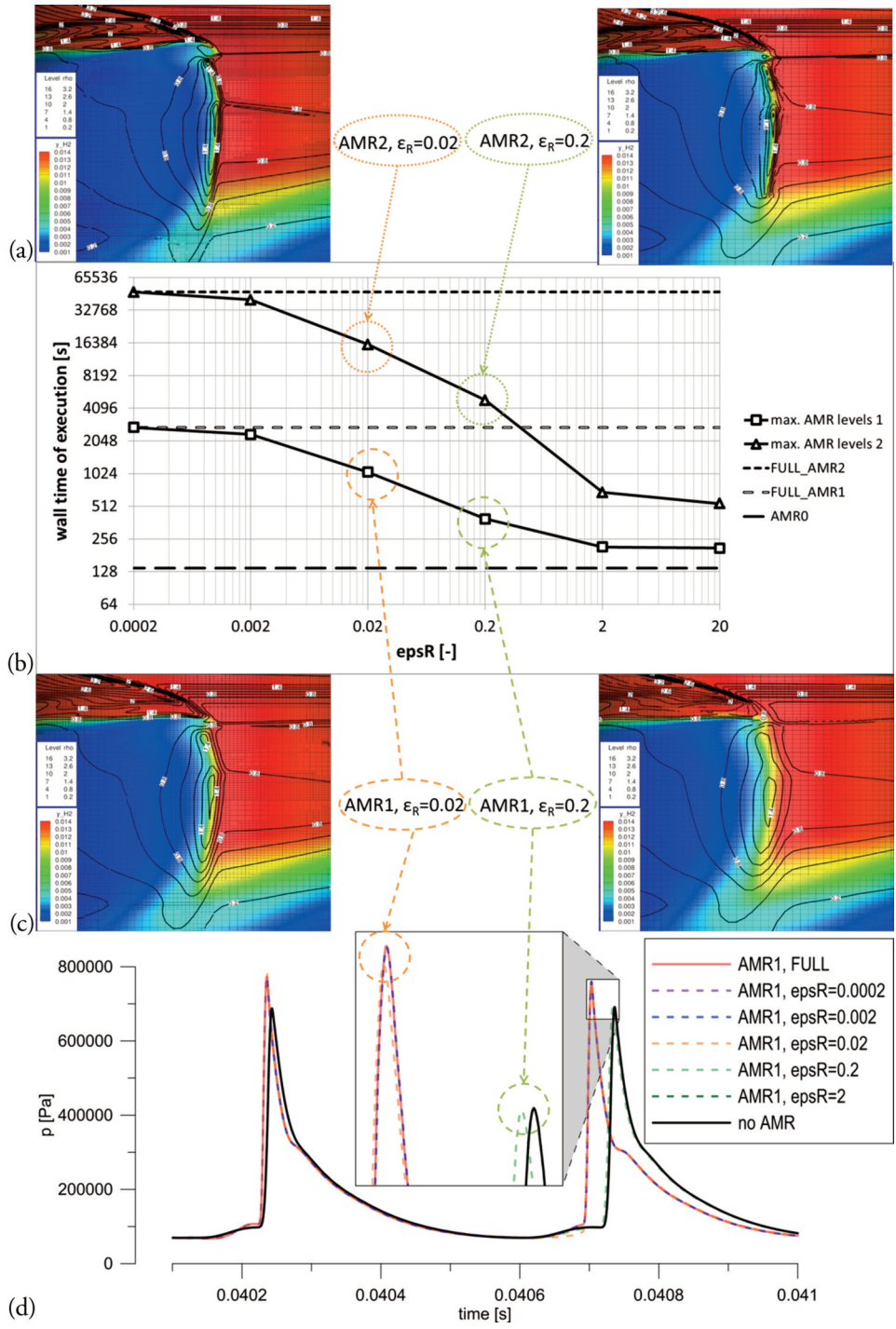

Fig. 34. Comparison of performance and accuracy of refinement thresholds. Isolines of density and contours of mass concentration of hydrogen near the detonation wave for (a) two and (c) one AMR levels allowed. The main flow direction is from top to bottom. (b) Wall time execution for various refinement thresholds. (d) Pressure history at sensor for various refinement thresholds and one AMR level allowed.

6. CONCLUSIONS

In this work authors described the complete simulation model that can be successfully applied to simulations of the Rotating Detonations Engine. Results of simulations are compared with experimental data. It was demonstrated that the first- and second-order shock capturing techniques, model of inviscid, reactive and compressible gas offer the acceptable accuracy for the purpose of the rotating detonation simulations for propulsion applications. Additionally, authors demonstrated that Adaptive Mesh Refinement technique can be successfully used in simulations of the RDE and greatly contribute to the improvement of the performance of simulations, which is crucial if simulation results are to be used in the design process of the engine.

Using the developed numerical approach, the flow field of the RDE combustion chamber has been investigated (details are described in the work of Folusiak and Swiderski), focusing on a representative geometry and flow conditions. The results show that:

- rotating detonation is quite easily obtained in various geometries and for a wide range of the inlet and outlet conditions,
- detonation front is usually located very close to the fuel inlet (10-15 mm), where the fuel-air mixing is efficient enough to create stoichiometric mixture,
- detonation wave can propagate in a mixture with non-uniform composition,
- detonation can be obtained for flows with supersonic flow behind the throat and for subsonic flows without the critical flow as well,
- the final number of detonation wave fronts depends both on the mixture composition and wave propagation stability.

It was shown that for low pressure ratios (1.2-2) between the inlet and outlet of the chamber a stable propagation is possible. However, significant losses can be expected because of strong series of shock waves observed at the expansion section of the RDE. Additionally, the calculated outflow temperature has very high values (can be above 2000 K for stoichiometric air-hydrogen mixtures). From aforementioned reasons it is concluded that the better mode of operation of the RDE combustion chamber is supersonic mode. It is possible to obtain a very stable detonation wave for pressure ratios in the range of 3-4 and the impact of the detonation wave both on inlet and outlet conditions is then negligible. For these conditions, flow behind the detonation wave relatively quickly expands azimuthally and axially.

Acknowledgments

The authors want to express their thanks and gratitude to Prof. Piotr Wolanski, for scientific and technical leadership throughout the project. True appreciation for our former colleagues involved in RDE works, namely Dr Arkadiusz Kobiera, Prof. Jan Kindracki, Dr Pawel Surmacz, Dr Grzegorz Rarata,, Dr Borys Lukasik, Dr Dominik Kublik, Kamil Sobczak and Dr Michal Kawalec.

REFERENCES

[1] Kindracki, J., Wolanski, P. and Gut, Z., 2011, "Experimental research on the rotating detonation in gaseous fuels-oxygen mixtures," Shock Waves, **21**(2), pp. 75-84. 10.1007/s00193-011-0298-y.

[2] Shao, Y.-T., Liu, M. and Wang, J.-P., 2010, "Numerical Investigation of Rotating Detonation Engine Propulsive Performance," Combustion Science and Technology, **182**(11-12), pp. 1586-1597. 10.1080/00102202.2010.497316.

[3] Yetao, S., Meng, L. and Jianping, W., 2010, "Continuous Detonation Engine and Effects of Different Types of Nozzle on Its Propulsion Performance," Chinese Journal of Aeronautics, **23**(6), pp. 647-652. 10.1016/S1000-9361(09)60266-1.

[4] Liu, S.-J., Lin, Z.-Y., Sun, M.-B. and Liu, W.-D., 2011, "Thrust Vectoring of a Continuous Rotating Detonation Engine by Changing the Local Injection Pressure," Chinese Physics Letters, **28**(9), p. 094704. 10.1088/0256-307x/28/9/094704.

[5] Liu, M., Zhou, R. and Wang, J.-P., 2011, "Three-dimensional simulation of rotating detonation engines," presented at the IWDE, Tokyo.

[6] Davidenko, D. M., Gökalp, I. and Kudryavtsev, A. N., 2007, "Numerical simulation of the continuous rotating hydrogen-oxygen detonation with a detailed chemical mechanism," Moscow, Russia, pp. 19-22, Available:
http://wehsff.imamod.ru/pages/Section 6 Propulsion Physics, Airbreathing Propulsion/Kudryavtsev.pdf

[7] Davidenko, D. M. et al., 2009, "Continuous detonation wave engine studies for space application," Progress in Propulsion Physics, vol. **1**, pp. 353-366. 10.1051/eucass/200901353.

[8] Davidenko, D. M., Eude, Y., Gökalp, I. and Falempin, F., 2011, "Theoretical and Numerical Studies on Continuous Detonation Wave Engines," presented at the *17th AIAA International Space Planes and Hypersonic Systems and Technologies Conference*, San Francisco, California. 10.2514/6.2011-2334.

[9] Davidenko, D. M., Gökalp, I. and Kudryavtsev, A. N., 2008, "Numerical Study of the Continuous Detonation Wave Rocket Engine," presented at the *15th AIAA International Space Planes and Hypersonic Systems and Technologies Conference*, Dayton, OH. 10.2514/6.2008-2680.

[10] Hayashi, A. K. et al., 2009, "Sensitivity Analysis of Rotating Detonation Engine with a Detailed Reaction Model," presented at the *47th AIAA Aerospace Sciences Meeting including The New Horizons Forum and Aerospace Exposition*, Orlando, Florida. 10.2514/6.2009-633.

[11] Hishida, M., Fujiwara, T. and Wolanski, P., 2009, "Fundamentals of rotating detonations," Shock Waves, **19**(1), pp. 1-10. 10.1007/s00193-008-0178-2.

[12] Kindracki, J., Kobiera, A., Wolanski, P., Gut, Z., Folusiak, M. and Swiderski, K., 2011, "Experimental and numerical study of the rotating detonation engine in hydrogen-air mixtures," Progress in Propulsion Physics, vol. **2**, pp. 555-582. 10.1051/eucass/201102555.

[13] Folusiak, M., Swiderski, K., Kobiera, A. and Wolanski, P., 2009, "Three-dimensional modeling of the Rotating Detonation Engine," presented at the *22nd International Colloquium on the Dynamics of Explosions and Reactive Systems*, Minsk, Belarus.

[14] Yi, T.-H., Lou, J., Turangan, C., Khoo, B. C. and Wolanski, P., 2010, "Effect of Nozzle Shapes on the Performance of Continuously Rotating Detonation Engine," presented at the *48th AIAA Aerospace Sciences Meeting Including the New Horizons Forum and Aerospace Exposition*, Orlando, Florida. 10.2514/6.2010-152.

[15] Schwer, D. and Kailasanath, K., 2010, "Numerical Investigation of Rotating Detonation Engines," in *46th AIAA/ASME/SAE/ASEE Joint Propulsion Conference & Exhibit*, 0 vols., American Institute of Aeronautics and Astronautics.

[16] Schwer, D. and Kailasanath, K., 2012, "Feedback into Mixture Plenums in Rotating Detonation Engines," in *50th AIAA Aerospace Sciences Meeting including the New Horizons Forum and Aerospace Exposition*, 0 vols., American Institute of Aeronautics and Astronautics.

[17] Nordeen, C. A., Schwer, D., Schauer, F., Hoke, J., Barber, T. and Cetegen, B. M., 2011, "Energy Transfer in a Rotating Detonation Engine," in *47th AIAA/ASME/SAE/ASEE Joint Propulsion Conference & Exhibit*, 0 vols., American Institute of Aeronautics and Astronautics.

[18] Nordeen, C. A., Schwer, D., Schauer, F., Hoke, J., Barber, T. and Cetegen, B. M., 2016, "Role of inlet reactant mixedness on the thermodynamic performance of a rotating detonation engine," Shock Waves, **26**(4), pp. 417-428. 10.1007/s00193-015-0570-7.

[19] Schwer, D. and Kailasanath, K., 2013, "Fluid dynamics of rotating detonation engines with hydrogen and hydrocarbon fuels," Proceedings of the Combustion Institute, **34**(2), pp. 1991-1998. 10.1016/j.proci.2012.05.046.

[20] Wolanski, P., 2013, "Detonative propulsion," Proceedings of the Combustion Institute, **34**(1), pp. 125-158. 10.1016/j.proci.2012.10.005.

[21] Wolanski, P., 2015, "Application of the Continuous Rotating Detonation to Gas Turbine," Applied Mechanics and Materials, vol. **782**, pp. 3-12, 10.4028/www.scientific.net/AMM.782.3.

[22] Wolanski, P. et al., 2018, Development of Gasturbine with Detonation Chamber. In: Li, J.M., Teo, C., Khoo, B., Wang, J.P., Wang, C. (eds) Detonation Control for Propulsion. Shock Wave and High Pressure Phenomena. Springer, Cham, pp. 23-37. Chap. 2. 10.1007/978-3-319-68906-7_2.

[23] Swiderski, K., 2013, "Numerical modeling of the rotating detonation combustion chamber," PhD Thesis, WUT, Warsaw.

[24] Berger, M. J. and Oliger, J., 1984, "Adaptive mesh refinement for hyperbolic partial differential equations," Journal of Computational Physics, **53**(3), pp. 484-512. 10.1016/0021-9991(84)90073-1.

[25] Vollmer, D. B., 2003, "Adaptive mesh refinement using subdivision of Unstructured elements for conservation laws," MSc Thesis, University of Reading.

[26] Lian, Y., Hsu, K., Shao, Y., Lee, Y., Jeng, Y. and Wu, J., 2006, "Parallel adaptive mesh-refining scheme on a three-dimensional unstructured tetrahedral mesh and its applications," Computer Physics Communications, **175**(11-12), pp. 721-737. 10.1016/j.cpc.2006.05.010.

[27] Azevedo, J. L. F. and Korzenowski, H., 2009, "An assessment of unstructured grid finite volume schemes for cold gas hypersonic flow calculations," Journal of Aerospace Technology and Management, **1**(2), pp. 135-152.

[28] Ripley, R. C., Lien, F.-S. and Yovanovich, M. M., 2004, "Adaptive Unstructured Mesh Refinement of Supersonic Channel Flows," International Journal of Computational Fluid Dynamics, **18**(2), pp. 189-198. 10.1080/10618560310001634168.

[29] Ito, K. Kunugi, T. and Ohshima, H., 2010, Development and Verification of Unstructured Adaptive Mesh Technique with Edge Compatibility, Journal of Power and Energy Systems, vol. **4**, pp. 72-83. 10.1299/jpes.4.72.

[30] Berger, M. J. and Colella, P., 1989, "Local adaptive mesh refinement for shock hydrodynamics," Journal of Computational Physics, **82**(1), pp. 64-84. 10.1016/0021-9991(89)90035-1.

[31] Boden, E. F., 1997, "An adaptive gridding technique for conservation laws on complex domains," PhD thesis, Cranfield University.

[32] Mavriplis, D. J., 1995, "Multigrid techniques for unstructured meshes," NASA Contractor Report 195070, Institute for Computer Applications in Science and Engineering, NASA Langley Research Center, Hampton, VA.
Available: https://apps.dtic.mil/dtic/tr/fulltext/u2/a294610.pdf

[33] Berger, M. J., 1987, "On Conservation at Grid Interfaces," SIAM Journal on Numerical Analysis, vol. **24**, p. 967. 10.1137/0724063.

[34] Folusiak, M., 2013, "Development of simulation methods of rotating detonation in complex geometries," PhD thesis, Warsaw University of Technology, Warsaw.

[35] Liang, Z., Browne, S., Deiterding, R. and Shepherd, J. E., 2007, "Detonation front structure and the competition for radicals," Proceedings of the Combustion Institute, **31**(2), pp. 2445-2453. 10.1016/j.proci.2006.07.244.

[36] Lu, T., Law, C. K. and Ju, Y., 2003, "Some aspects of chemical kinetics in chapman-jouguet detonation: Induction length analysis," Journal of Propulsion and Power, **19**(5), pp. 901-907.
[37] Petersen, E. L. and Hanson, R. K., 1999, "Reduced kinetics mechanisms for ram accelerator combustion," Journal of propulsion and power, **15**(4), pp. 591-600.
[38] Petersen, E. L., Davidson, D. F. and Hanson, R. K., 1999, "Ignition delay times of ram accelerator CH4/O2/diluent mixtures," Journal of Propulsion and Power, **15**(1), pp. 82-91.
[39] Folusiak, M., Swiderski, K., Kobiera, A. and Wolanski, P., 2009, "Two-dimensional modeling of the rotating detonation with fuel injection," presented at the *European Conference for AeroSpace Sciences*, Versailles, France.
[40] Wolanski, P., 2011, "Rotating detonation wave stability," presented at the *23rd International Colloquium on the Dynamics of Explosions and Reactive Systems*, University of California, Irvine, USA.
[41] Eude, Y., Davidenko, D. and Izrar, B., 2011, "Simulation of continuous detonation in H2-O2 mixture using adaptive mesh refinement," presented at the *20ème Congrès Franccais de Mécanique*, France. Available: http://documents.irevues.inist.fr/handle/2042/46347.

MODELOWANIE NUMERYCZNE SILNIKA Z WIRUJĄCĄ DETONACJĄ

Abstrakt

Pomysł wykorzystania zjawiska wirującej detonacji do napędu był po raz pierwszy rozważany w latach pięćdziesiątych ubiegłego wieku przez zespoły badawcze Adamsona i Nichollsa na Uniwersytecie Michigan. Badania nad silnikiem z detonacyjną komorą spalania zostały wznowione po blisko 40 latach i dziś prace prowadzone są w wielu jednostkach naukowych na świecie, a w Polsce na Politechnice Warszawskiej od 2004 roku. W latach 2010-2014 Instytut Lotnictwa oraz Politechnika Warszawska wspólnie realizowały projekt w ramach Programu Operacyjnego Innowacyjna Gospodarka 'Silnik Turbinowy z detonacyjną komorą spalania'. Projekt zakłada zastąpienie komory spalania turbowałowego silnika GTD-350 pierścieniową komorą detonacyjną.

Artykuł skupia się na badaniach numerycznych wpływu geometrii oraz parametrów przepływu na strukturę i stabilność propagacji wirującej detonacji. Przedstawione wyniki są w większości wynikiem prac autorów nad rozwojem kodu REFLOPS USG w czasie trwania projektu i koncentruje się na rozwoju i implementacji wysokowydajnych metod symulacji silnika z detonacyjną komorą spalania oraz ich zastosowaniu w symulacjach numerycznych propagacji wirującej fali detonacyjnej w silniku RDE.

Słowa kluczowe: silnik RDE, CFD, wirująca detonacja, modelowanie numeryczne.